MÖSSBAUER EFFECT STUDIES OF SOME IRON SALTS

by

Vo van Thanh

A thesis submitted to
the Board of Graduate Studies
in partial fulfilment of the requirements for the degree of
Master of Science.

Department of Physics
Sir George Williams University
Montreal

September 1969

TABLE OF CONTENTS

ABSTRACT

Using the Mössbauer effect as a tool, the isomer shifts and quadrupole splittings of four iron salts have been measured. The salts are : formamide ($FeCl_2.2HCONH_2$) and N-Methylformamide ($FeCl_2.2HCONHCH_3$) iron halide complexes, the ferrocene acetonitrile ($Fe(CH)_9CCH_2CN$) and its titanium derivative ($Fe(CH)_9CCH_2CNTiCl_4$). The experimental data of the Mössbauer spectra were analyzed with the help of a curve-fitting computer program using the method of least-squares fitting. The results from the study of the iron halide complexes suggested that they are high-spin ferrous compounds and may possess a tetrahedral configuration. The ferrocene acetonitrile and its titanium derivative are believed to be low-spin ferrous compounds, the existence of the quadrupole splitting in the ferrocene acetonitrile is interpreted as resulting from a strong deformation by the ligands to which the Fe atom is bound.

ACKNOWLEDGEMENTS

The author wishes to thank Dr. S.K. Misra whose supervision, advice and interest has made this thesis possible. The author also appreciates the encouragement received from Dr. R.C. Sharma and would like to thank Mr. J. Blaison for his helpful technical assistance.

CHAPTER I

INTRODUCTION

The subject of this thesis is an experimental study of some iron complexes using the Mössbauer effect as a tool. The recoilless fractions of emission and absorption of gamma radiation are considerable for Fe^{57} even at room temperature. The experiments were therefore carried out at room temperature in the hope that much could be learned at this temperature.

The recoilless emission and absorption of gamma radiation was discovered in 1957 by R.L. MÖSSBAUER (1,2). It is briefly as follows. Under suitable conditions, to be discussed in Chapter III, the entire crystal, in which the Mössbauer emitter (or absorber) is embedded, rather than the nucleus alone participates in the sharing of the momentum received during the emission (or absorption) of a gamma ray photon. Since the mass of the crystal is much larger compared to that of the emitting nucleus, the recoil energy is almost reduced to zero. The Doppler broadening then disappears and the gamma ray energy lines are characterized by the natural line width. Thus, when the Mössbauer effect occurs, the gamma ray fluorescence technique becomes an extremely sensitive tool to measure very small energy shifts; it is

possible to measure energy differences between emission and absorption lines by changing the energy of any one of them by the Doppler effect. Since the lines now have natural shapes, the resonance is very sensitive even to very small energy differences. From the knowledge of the Doppler velocity, the energy differences can be calculated. A comparison of the calculated values, which depend on unknown parameters, with the experimental values provides useful information about the parameters involved.

Due to its versatility, the Mössbauer effect finds application not only in nuclear physics, where it was discovered, but also in many other fields, for example, solid state physics, relativity, chemistry, biophysics etc... The Mössbauer effect also enables one to separate various lines in a Zeeman spectrum thereby making it possible to study the polarization of the gamma ray photons.

A typical Mössbauer effect experiment basically consists of the following parts: (i) a source of Mössbauer radiation, (ii) an appropriate absorber, (iii) gamma radiation detection equipment and (iv) a velocity drive. For the experimental study reported in this thesis a Co^{57} source embedded in copper was used. It gave an unsplit Mössbauer radiation of 14.4 kev gamma rays. Details on the absorbers, the gamma ray counting system and the

velocity spectrometer are given in Chapter II. The resultant spectra were analyzed with the help of the computer to give a least-squares fit to the experimental data. The computer program used is given in the Appendix. The absorption line areas, location of the peaks and final widths at half maximum were determined and the relevant properties were then deduced. This is discussed in detail in Chapter IV with reference to the particular complexes investigated.

CHAPTER II

EXPERIMENTAL PROCEDURE

Figure 1 illustrates the simplest example of a resonant absorption experiment. Both source and absorber exhibit unsplit lines. These lines are Lorentzian and expressed by the Breit-Wigner formula

$$I(E) = \frac{\Gamma}{2\pi} \frac{1}{(E-E_o)^2 + (\Gamma/2)^2} \quad , \tag{1}$$

where E_o is the transition energy between the excited and ground states and Γ is the full width of the distribution at half maximum. They can also be of Gaussian shape :

$$J(E) = \exp\left[-\left(\frac{E-E_o}{\Gamma/2\sqrt{\ln 2}}\right)^2\right] \quad , \tag{2}$$

if there is sufficient interaction of the emitting or absorbing nuclei with the environment.

When the source and absorber are at rest, the emission and absorption lines overlap completely and a maximum of absorption is obtained; there is a minimum of transmitted intensity. When the source moves toward the absorber, the gamma ray energies increase, causing a shift of the emission line with regard to the absorption line, the overlapping area becomes smaller; the absorption decreases and the counter detects more counts. The

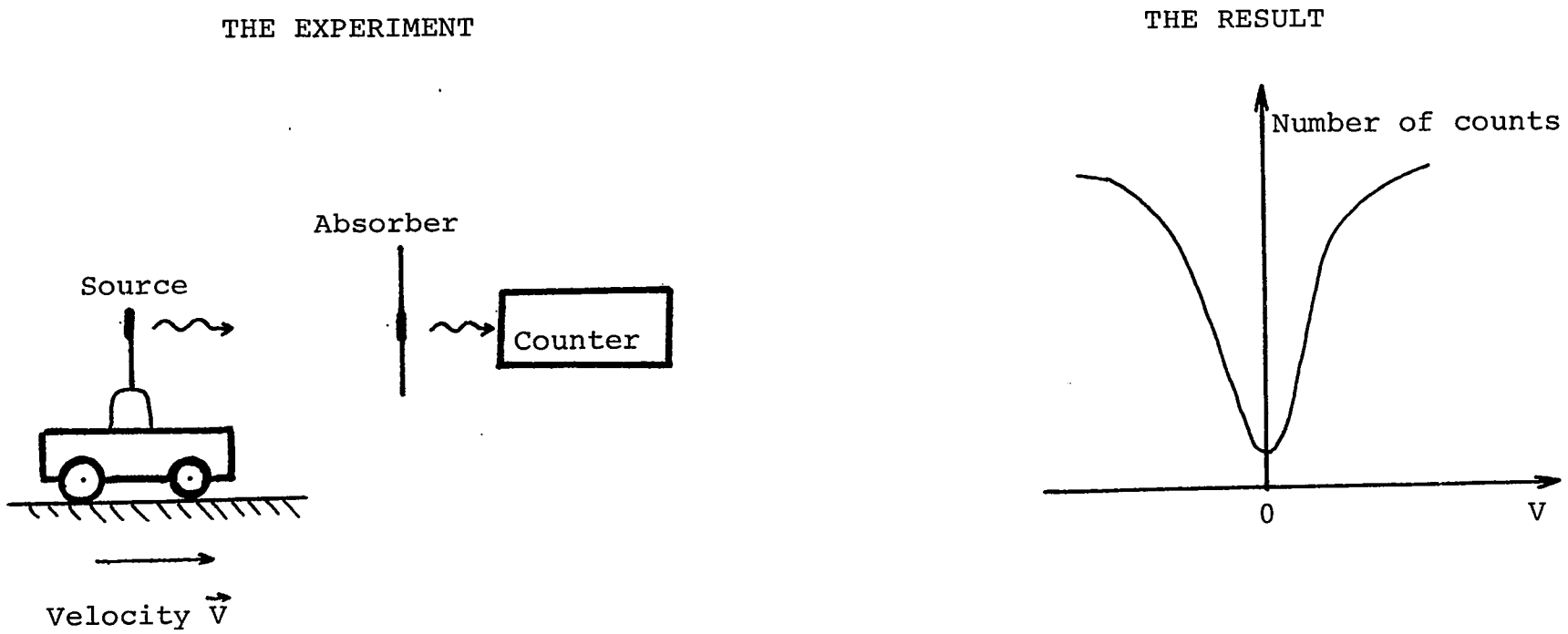

Fig.1 Resonant absorption experiment.

effect will be the same when the source moves backward with respect to the absorber. Therefore, the Mössbauer spectrum registered by the counter is symmetrical with regard to the zero velocity centre. The width of the Mössbauer spectrum is 2Γ ,being the fold of the two emission and absorption lines of equal width Γ . That the Mössbauer spectra are very sensitive even to extremely small Doppler speeds is exhibited by the fact that, in the case of Zn^{67}, an amplitude of few times 10^{-8} cm may be sufficient to destroy resonance.

The components of a Mössbauer experiment equipment consist of a radioactive source, a radiation detection system and a Mössbauer velocity spectrometer. They are briefly described as follows.

2.1. Source and absorber

Sources used in Mössbauer experiments are essentially solid. Their strength varies from some tens of millicuries up to about 0.4 curie(3). A source is characterized by its half-life, its fraction of recoil-less emission and its "monochromatism". A large recoil free emission is related to a high effective Debye temperature, Θ_D' ,defined as (4):

$$\Theta_D' = \Theta_D \left(M_{host} / M_{imp} \right)^{1/2} \qquad (3)$$

where Θ_D is the classical Debye temperature, M_{host} and M_{imp} represent respectively the atomic masses of the host atom and source atom. In an experiment where an unsplit gamma radiation is required, care must be exercised so that the location of the source at a particular lattice and in a particular host material may not bring a splitting of the radiation.

Co^{57} becomes the most commonly used source in Mössbauer experiments due to its large Lamb-Mössbauer factor (sect.3.1.) at room temperature and its wide range of compounds. The source used in our experiments is a 40mc Co^{57} prepared by Nuclear Science and Engineering Corporation, Pittsburgh at the Oak Ridge National Laboratory by irradiation and further chemical purification. It was annealed in copper at high temperature to avoid possible defects in the crystal lattice and exhibits an unsplit line of 14.4kev. At room temperature, the recoilless emission factor is about 80%. Figure 2 shows the decay of Co^{57} to the ground state of Fe^{57}. Only 9% of the radiation emitted by the 137 kev level goes directly to the ground state of Fe^{57}, the remaining 91% goes to the 14.4 kev state. There is,therefore, a strong background of 122.6 kev gamma rays, but these gamma rays are easily eliminated by the use of a proper window in the single channel analyser (S.C.A.)(Figure 3).

Because of the metallic host matrix, the emission line is not centered exactly at 14.4 kev but undergoes an isomer shift (sect.3.2). With respect to an absorber of sodium nitroprusside ($Na_2(Fe(CN)_5NO).2H_2O$) at room temperature, the Co^{57} source embedded in copper exhibits an isomer shift of 0.483 mm/s (Here the energy shift is represented by the Doppler velocity of the source relative to the absorber). All the results reported in this thesis will be expressed relative to sodium nitroprusside by taking this shift into account.

The iron salts which constitute the absorbers in our experiments are two iron halide complexes of the type $FeCl_2.2L$ (L= $HCONH_2$, $HCONHCH_3$) and ferrocene acetonitrile ($Fe(CH)_9CCH_2CN$) with its titanium derivative ($Fe(CH)_9CCH_2CNTiCl_4$). The iron halide complexes are prepared by the reaction of iron carbonyls with various ligands in chloroform as solvent (5); the magnetic susceptibility measurements and infrared spectral study suggest that these complexes have tetrahedral configuration which corresponds to a weak ligand field (5).

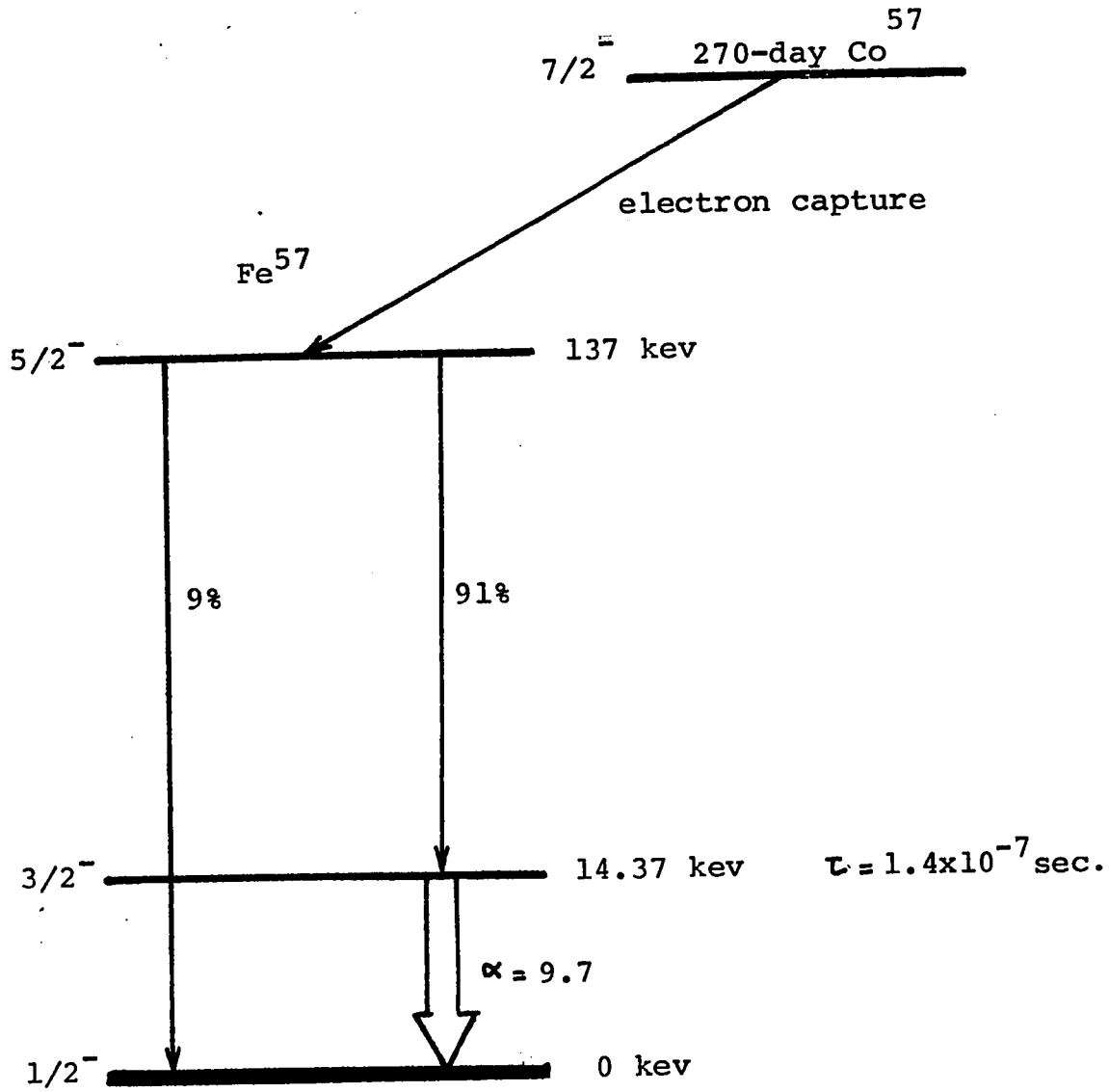

Fig. 2 Decay scheme of Fe^{57}

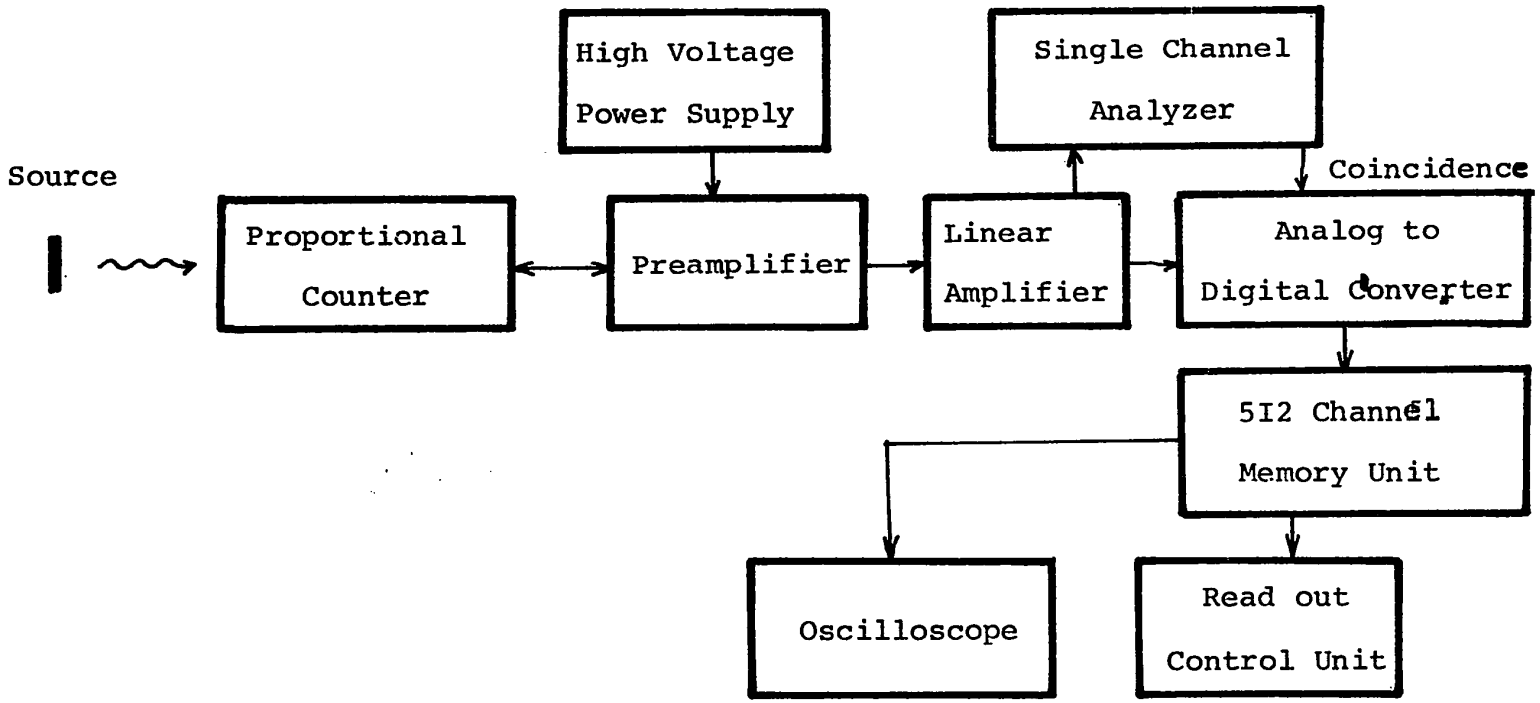

Fig.3 Block diagram for pulse-height measurement and window adjustment(S.C.A.)

2.2. Detection equipment.

PROPORTIONAL COUNTER : One of the principal factors which determine the quality of a Mössbauer spectrum is the choice of the detector. Gamma rays of energy below 20 kev, as in the case of Fe^{57}, can hardly penetrate a scintillation counter. Due to its high resolution and satisfactory efficiency, the proportional counter is the most appropriate for Mössbauer experiments. The solid state detectors also find their use in special cases, as for example, when a very high energy resolution is required. Whereas the proportional counter can be used at room temperature, the solid state detectors require low temperatures for their use. Figure 4 displays a pulse height spectrum (P.H.S.) of the Co^{57} source. The type of proportional counter used is AMPIREX 303PC filled with a 90%Kr-10%CH_4 mixture at a pressure of 38mm of Hg. The spectrum shows a strong 6 kev X-ray background resulting from the photoelectric effect which is produced by the scattering of 14.4 kev gamma rays by the environment.

The cross section of the 6 kev gamma ray is about 6 barns and the surface density of the counter is approximately 5×10^{-2}g/cm^2. The efficiency of the proportional counter is then

$$\epsilon = N\rho\frac{Z}{A}\sigma = 6\times10^{23}\times5\times10^{-2}\times\frac{26}{57}\times6\times10^{-24} \simeq 10\%$$

From Fig. 4, the energy resolution is

$$R = \frac{\Delta E}{E} = \frac{22}{97} \approx 23\%$$

where ΔE is the half-width at half maximum of the 6 kev peak and E is the corresponding energy of the peak, both values are expressed in number of channels.

PREAMPLIFIER (ORTEC Model 109). This preamplifier is designed for semiconductor detectors but can be used in almost any application where very low noise amplification is desired such as proportional counters.

LINEAR AMPLIFIER (HP Model 5582A) & SINGLE CHANNEL ANALYZER (HP Model 5583A). The Hewlett-Packard Model 5582A Linear Amplifier provides maximum flexibility for nuclear pulse counting with all types of detectors and with a wide range of counting rates. This linear amplifier is an ideal input for the HP5583A Single Channel Analyzer in nuclear pulse analysis applications.

ANALYZER SYSTEMS (ND-180F and ND-180M). These consist of two units. The F Unit which is an Analog to Digital Converter and the M Unit which is a Memory Unit. The F Unit digitizes analog information from the linear amplifier so that it can be utilized by the M Unit. The M Unit is basically a digital computer, it contains a channel scaler with 512 channels and a Memory Register which can store up to 1,000,000 counts in each channel.

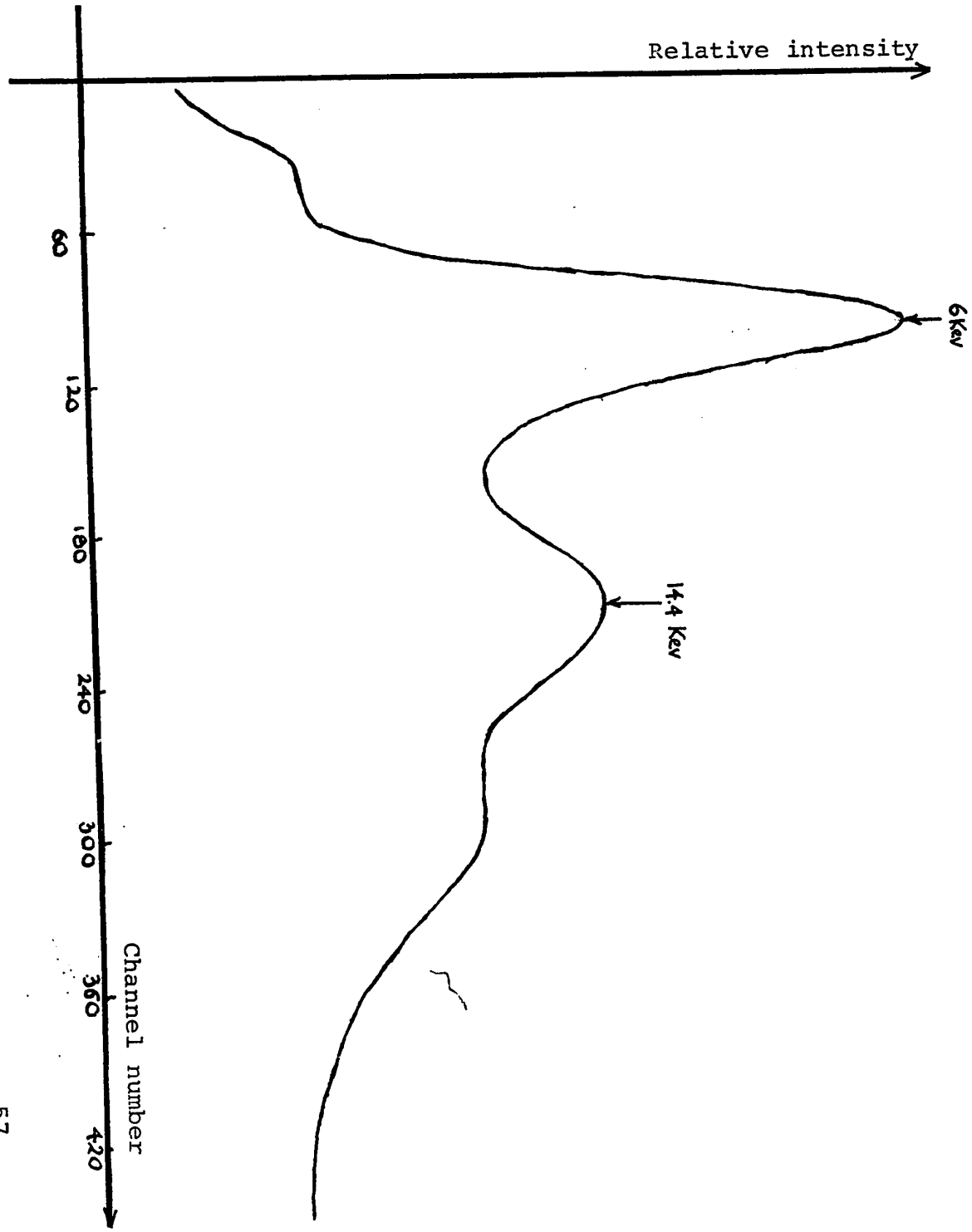

Fig. 4. Pulse-height spectrum of low energy gamma radiation from Fe^{57}

2.3. Mössbauer effect spectrometer.

The Mössbauer effect spectrometer is an apparatus which imparts a Doppler motion to the source. It also coordinates the counting rate at the detector so that any Mössbauer absorption or scattering spectrum will have its channel number as a function of the velocity of the source (Figure 5). The Model AM-1, manufactured by Nuclear Science and Engineering Corporation, consists of 3 basic units:

(i) The BASE PLATE : It is a solid Al plate which provides a very rigid structure on which all the mechanical parts, the transducer (on which the source is mounted), the absorber holder, the detector holder, and the Cryoflask (required only for low temperature experiments) are mounted.

(ii) The TRANSDUCER : It is a precision made electro-mechanical unit which provides a forward and retrograde motion to the source with constant acceleration (Figure 4). The operating frequency range is 15-50 cps and the velocity can vary between 0 and 60 cm/s by steps of 0.01 cm/s . The linearity precision of the triangular wave-form is about 1% over 95% of the half period of the velocity waveform.

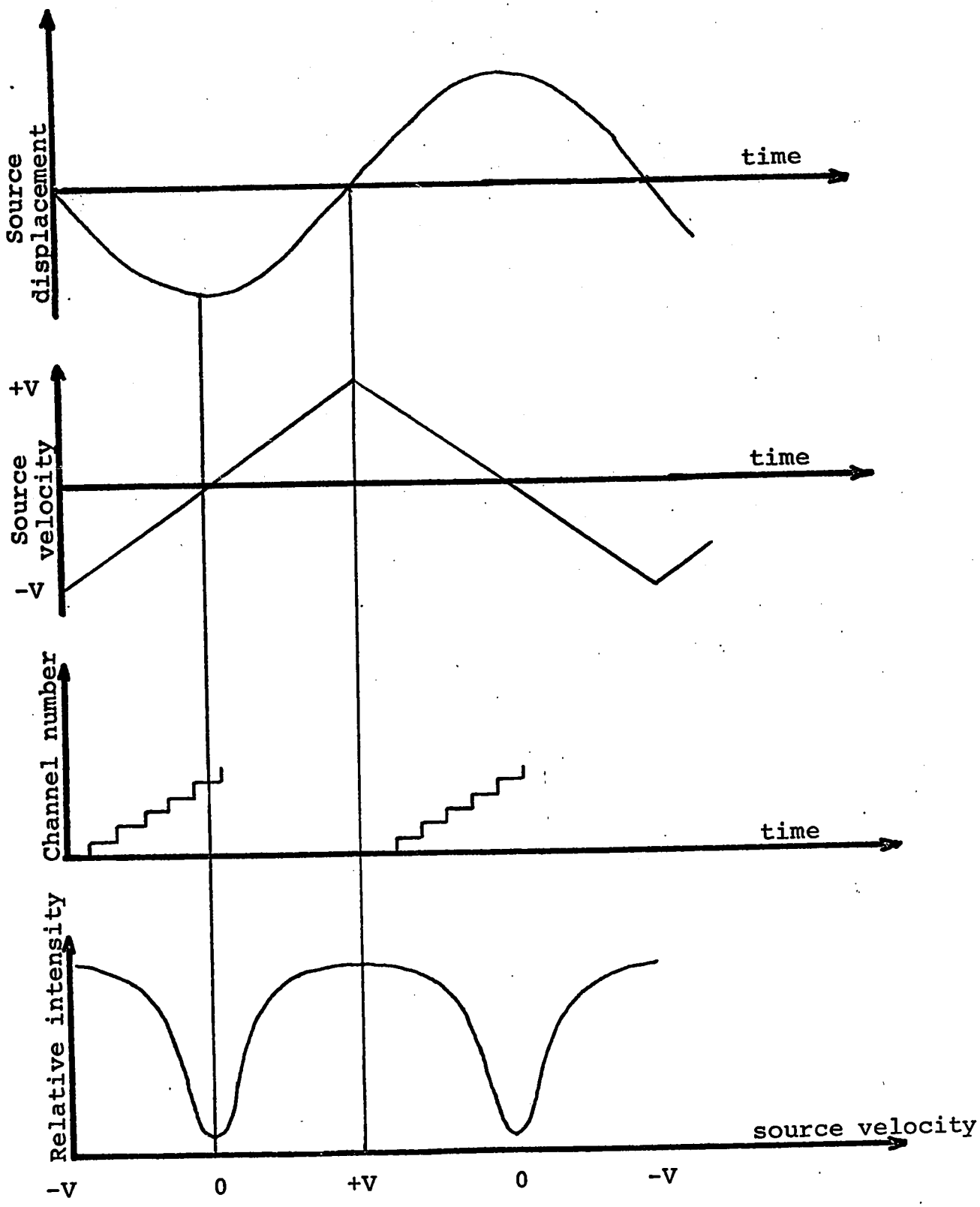

Fig. 5. Recording of a Mössbauer spectrum.

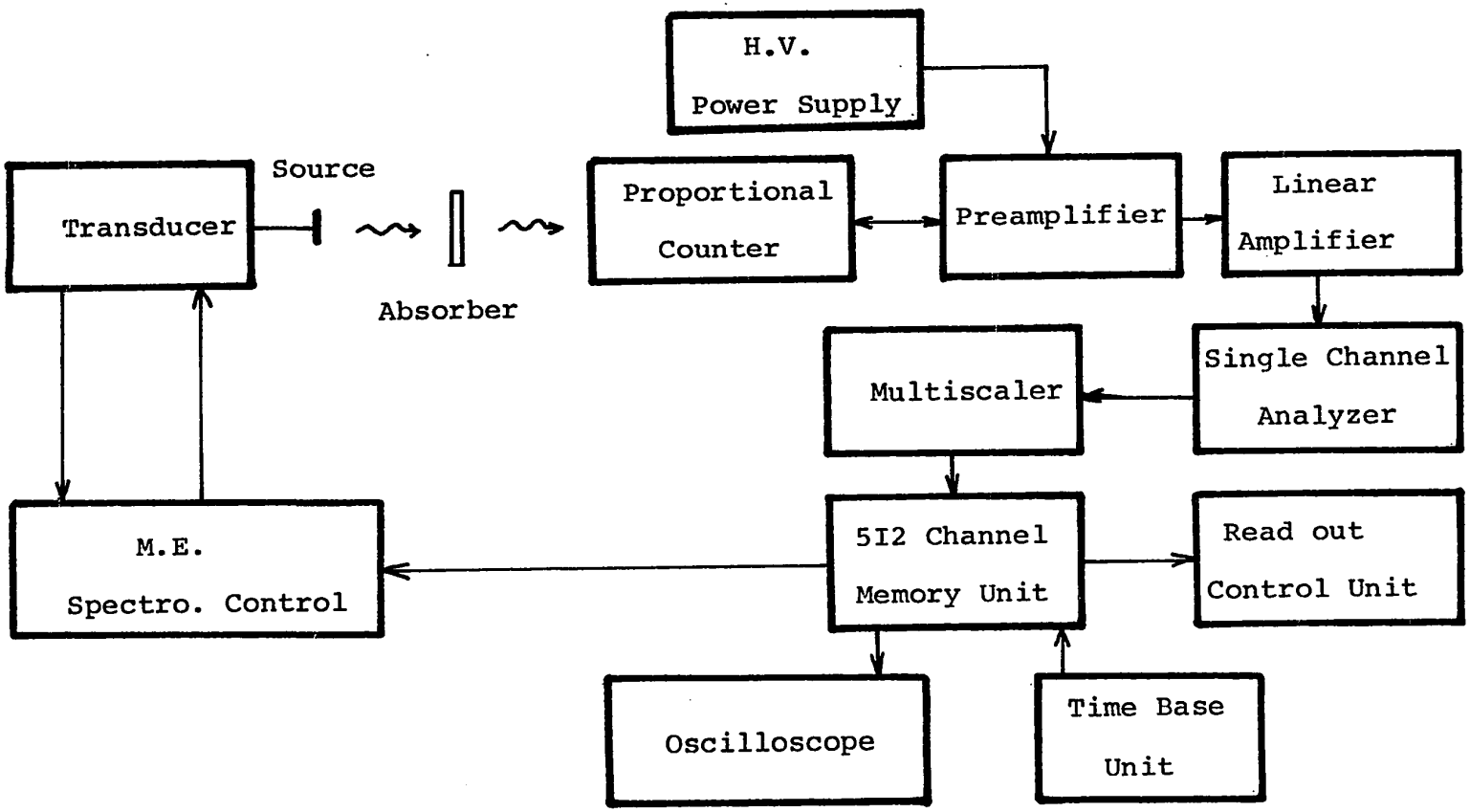

Fig.6 Block diagram of the Mössbauer effect experiment.

(iii) The CONTROL UNIT : It is an all-solid state electronic unit which accepts a square wave signal from the address register of a multi-channel analyzer (M.C.A.). It contains input signal idealizing circuitry, triangular function generating circuitry and the necessary servo and D.C. power amplifiers required to drive the transducer.

2.4. Experimental technique.

The source emits gamma rays of different energies depending on its velocity. The energy shift from the initial value E_o is

$$\Delta E = \frac{v}{c} E_o \qquad (E_o = 14.4 \text{ kev}), (4)$$

where v is the Doppler velocity of the source (positive when the source moves toward the absorber).

Part of these gamma rays are absorbed by a filter consisting of the same isotope as the source (Fe^{57} salts). The absorption occurs whenever the photon energy of the incoming beam is equal to the excitation energy of the iron nucleus in the salt molecule. The non-resonant gamma rays pass through the absorber and are transformed into pulses proportional in height to their energies by the proportional counter, these pulses are amplified by an amplification system consisting of a preamplifier and

a linear amplifier. A single channel analyzer selects the 14.4 kev gamma rays of the pulse spectrum of Co^{57}. Pulses coming from the single channel analyzer go through a multichannel analyzer operated in multiscaler mode. A time base generator is provided to open one channel after the other with constant intervals of time. The control-servo of the Mössbauer effect spectrometer adjusts each channel to a certain velocity of the source (or a certain gamma ray energy). A triangular waveform is used as a reference signal and the spectrum is displayed twice on the cathode ray tube of the analyzer; the second half is the mirror image of the first half of the spectrum. A diagrammatic explanation is provided in Figures 5 and 6.

In Mössbauer spectroscopy, the accuracy of the results is mostly concerned with the peak position, the peak height and the area of the lines in the spectrum. High precision of the peak position is particularly important in the detection of small shifts such as temperature or pressure shifts. Errors can result from irregularities in the motion of the source, excessive width of the Mössbauer absorption peak and the random process of radioactive decay (counting statistics). To test the linearity of the waveform of the spectrometer, the well-known six peaks of natural iron (2.19% isotopic abundance) are used. A curve fitting computer program (see Appendix) will be used to decide whether the line shape of the

absorption peak belongs to the Lorentzian or Gaussian distribution.

Mössbauer experiments usually deal with gamma-rays of energies below 100 kev, and X-ray background radiation often represents a disturbing factor. It comes from non-resonant 14.4 kev gamma-rays emitted with some recoil (B) (Figure7) and from electronic interaction between high energy gamma-rays and matter near the detector and in the absorber (B'). The quality of a Mössbauer spectrum is often characterized by the fraction effect :

$$\epsilon = \frac{B-(B-H)}{B+B'} = \frac{H}{B+B'} \qquad (5)$$

which can be increased by reducing the background B',

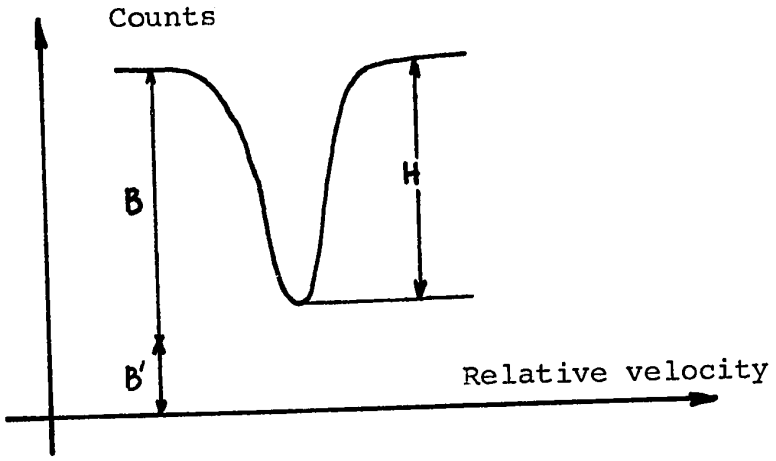

(H= peak height)

Fig.7 Background and peak height of a Mössbauer spectrum.

such as the strong 6 kev peak in Fig.4; a 5-mil Al foil provides an excellent filter of such radiation.

Distortion in the spectrum may be caused by the geometry of source, absorber and detector. Theoretically, the best geometry requires the absorber to be half way between the source and the detector. This configuration minimizes the detection of scattered Mössbauer radiation due to the reemission of absorbed gamma-rays. This last factor is considerably reduced when the counter has a large solid angle and when Mössbauer energy levels have large conversion coefficients(6). In practice best results are obtained when the absorber is closer to the detector than to the source. There are other sources of errors:the source area, the detector aperture, impurities in the counter,etc. These produce small errors compared to those mentioned above (7).

For a moving source, the counting rate is a function of the relative distance between the source and the detector. Necessary corrections are calculated and taken into account by the computer program (see Appendix).

CHAPTER III

THEORY

3.1. The Lamb-Mössbauer factors

Only a fraction f of the photons emitted by a source is without recoil. Similarly, a fraction f' of the n atoms of the absorber can absorb the Mössbauer radiation resonantly. These fractions f and f', which determine respectively the recoil free emission and absorption probabilities for the source and absorber, are referred to sometimes as Lamb-Mössbauer factors. Until the mechanism of line broadening is understood in detail, Mössbauer spectra are needed to deduce these f values.

The recoilless fraction for emission (or absorption) can be expressed in a first approximation by

$$\langle n_i | \exp(i\vec{k}.\vec{x}) | n_i \rangle \qquad (6)$$

where $\vec{k}$ is the wave vector of the gamma quantum, $\vec{x}$ is the time dependent coordinate of the centre of mass of the nucleus under investigation and $|n_i\rangle$ is the initial vibrational state of the lattice of the emitter(or absorber). In the case where the levels exhibit hyperfine structure by magnetic or quadrupole splittings (sect.3.2.,3.3.),it can be shown (8) that the total probability of Mössbauer effect during the nuclear transitions between the sublevels

of the first excited and ground levels of the nucleus remains the same as given by the expression (6).

In the Debye model of solids, the factor f is given by (1,9)

$$f = \exp(-2M) = \exp - \left\{ \frac{3R}{2k\Theta} \left[1 + 4 \left(\frac{T}{\Theta} \right)^2 \right] \int_0^{\Theta/T} \frac{x\,dx}{e^x + 1} \right\} \qquad (7)$$

$$\simeq \exp - \left\{ \frac{3R}{2k\Theta} \left[1 + \frac{2}{3} \left(\frac{\pi T}{\Theta} \right)^2 \right] \right\} \quad (T \ll \Theta) \qquad (8)$$

where R is the recoil energy, Θ is the Debye temperature and k is the Botzmann constant. The above equations show that even at $0^{\circ}K$, f is large only if the recoil energy is small compared to $k\Theta$ and it decreases with increasing T and becomes negligible when $T \gg \Theta$. Tabulations and plots of the integral in equation (7) are available in the literature (10,11).

Figure 8 displays the temperature dependence of f within the limits of two extreme transitions where the Mössbauer effect is observable.

The Lamb-Mössbauer factor is related to the absorption cross section by (12)

$$\sigma(E) = \frac{\lambda^2}{2\pi} \frac{2I+1}{2I_0+1} \frac{1}{1+\alpha} f_h \frac{(\Gamma/2)^2}{(E-E_0)^2 + (\Gamma/2)^2}$$

$$= \sigma_0 f_h \frac{(\Gamma/2)^2}{(E-E_0)^2 + (\Gamma/2)^2} \qquad (9)$$

where λ is the gamma wavelength, I and I_o are respectively the nuclear spins of the excited and ground states, α is the conversion coefficient and h is the relative abundance of the isotope in question. E_o will be different from the energy transition if there is a chemical shift.

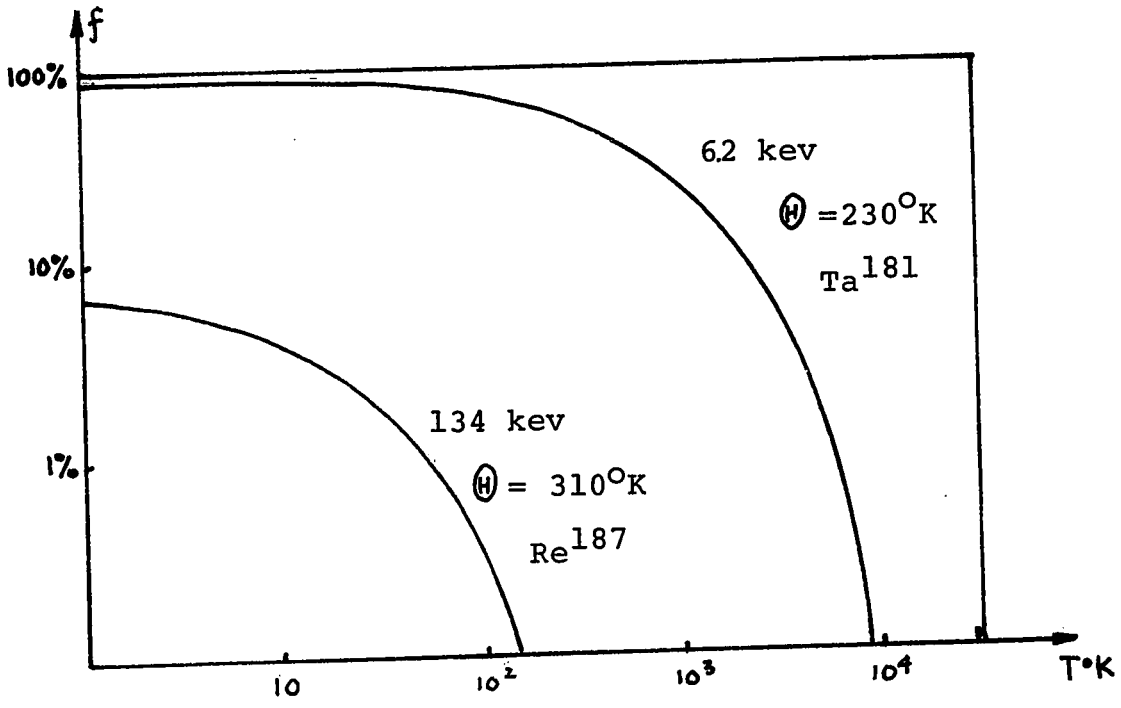

Fig. 8. The Lamb-Mössbauer factor for 2 representative gamma transitions.

For Fe^{57}, h = 2.2% to 100%

f = 90% at 0°K

= 80% at room temperature.

The maximum resonant absorption cross section is:

$$\sigma(E_o) = 3.6 \times 10^{-20} \text{ cm}^2 .$$

For all other non-resonant processes, the cross section is about $10^{-20}cm^2$.

The experimental determination of the quantities f and f' is accomplished by considering the area under the absorption peak of the Mössbauer spectrum. Calculations for a Lorentzian shape Mössbauer spectrum of full width at half maximum Γ_{exp} and peak dip p_{exp} lead to (13): Γ_a = apparent width, Γ' = absorber width,

$$\text{Area} = \pi \frac{c}{2E_0} \Gamma_{exp} \cdot p_{exp} \quad , \tag{10}$$

$$\text{with} \quad p_{exp} = \frac{\Gamma_a}{\Gamma_{exp}} f p(t) = \frac{2\Gamma h(t)}{\Gamma_{exp}} f p(t) \quad , \tag{11}$$

where t is the effective thickness of the absorber defined as $t = n\sigma_0 f'$, $h(t)$ and $p(t)$ are functions of t. For small t (or "thin" absorbers) (14):

$$0 \leq t \leq 5 \qquad p_{exp} = n\sigma_0 \frac{\Gamma}{\Gamma_{exp}} ff' [1 - 0.24t + 0.04t^2] \tag{12}$$

For large t

$$4 \leq t \leq 10 \qquad p_{exp} = 1.2 f \left[\frac{\Gamma}{\Gamma_{exp}} + 0.20 n\sigma_0 f' \frac{\Gamma}{\Gamma_{exp}} \right] \tag{13}$$

If f' is known from a separate experiment, for example, from a recoil-free Rayleigh scattering experiment (15), f can be deduced precisely from the

above equations, even if the natural emission line width Γ' is not known precisely. Otherwise, thin-absorber experiments may determine ff' and t, but not f and f' separately unless Γ' is known; but one usually has enough information on f to deduce f' from the product ff'.

3.2. Isomer shift

To understand the physical meaning of the isomer shift, let us consider two atoms having the same electronic shell, one of the nuclei is assumed to be a point, in the other the nuclear charge is distributed uniformly over a sphere of finite radius R_n. In the latter case, the binding energy of the atom is decreased; the energy levels are raised because some energy is gained in the expansion of the nucleus in the electronic field. If ΔE_B and ΔE_A are respectively the shifts corresponding to the excited state B and the ground state A (Fig.9a)the new transition energy is given by:

$$E_0' = E_0 + \Delta E_B - \Delta E_A$$

$$= E_0 + \frac{2}{5}\pi Z e^2 |\psi(0)|^2 \left[\langle r_B^2\rangle - \langle r_A^2\rangle\right] \qquad (15)$$

where $\langle r_A^2\rangle$ and $\langle r_B^2\rangle$ are the root mean square radii of states A and B and $|\psi(0)|^2$ is the non-relativistic s-electron density at the centre of the nucleus. $|\psi(0)|^2$ can be computed from a hydrogen-like wave function or more accurately from the

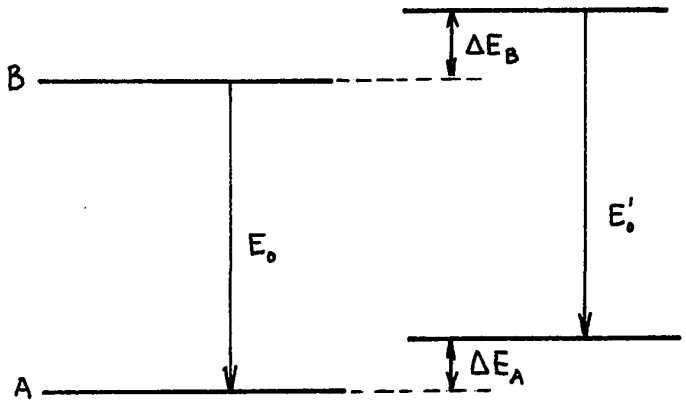

Fig.9a. Energy level shifts from point nucleus to finite size nucleus. Fig.9b gives an example of isomer shift in stainless steel.

Fermi-Segrè formula (16). Relativistic corrections for large Z are discussed by Shirley (17). Figure 10 shows a qualitative aspect of the relativistic correction as a function of Z.

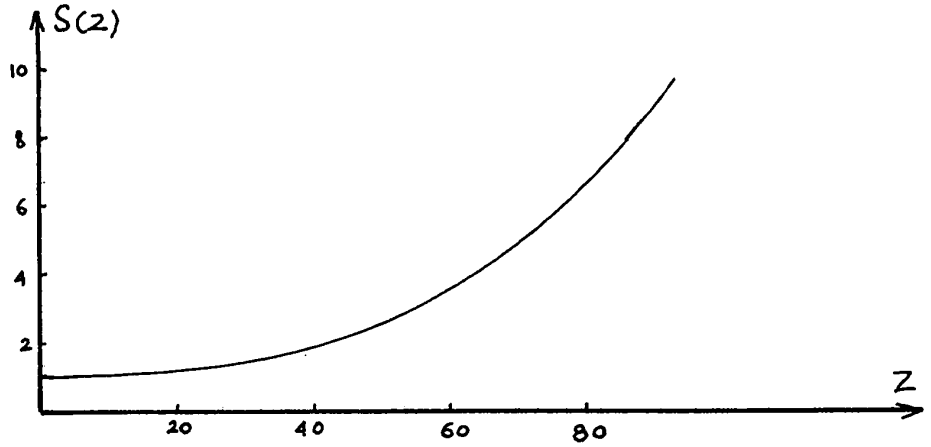

Fig.10. Relativistic correction of the magnitudes of the density of s-electrons on nuclei.

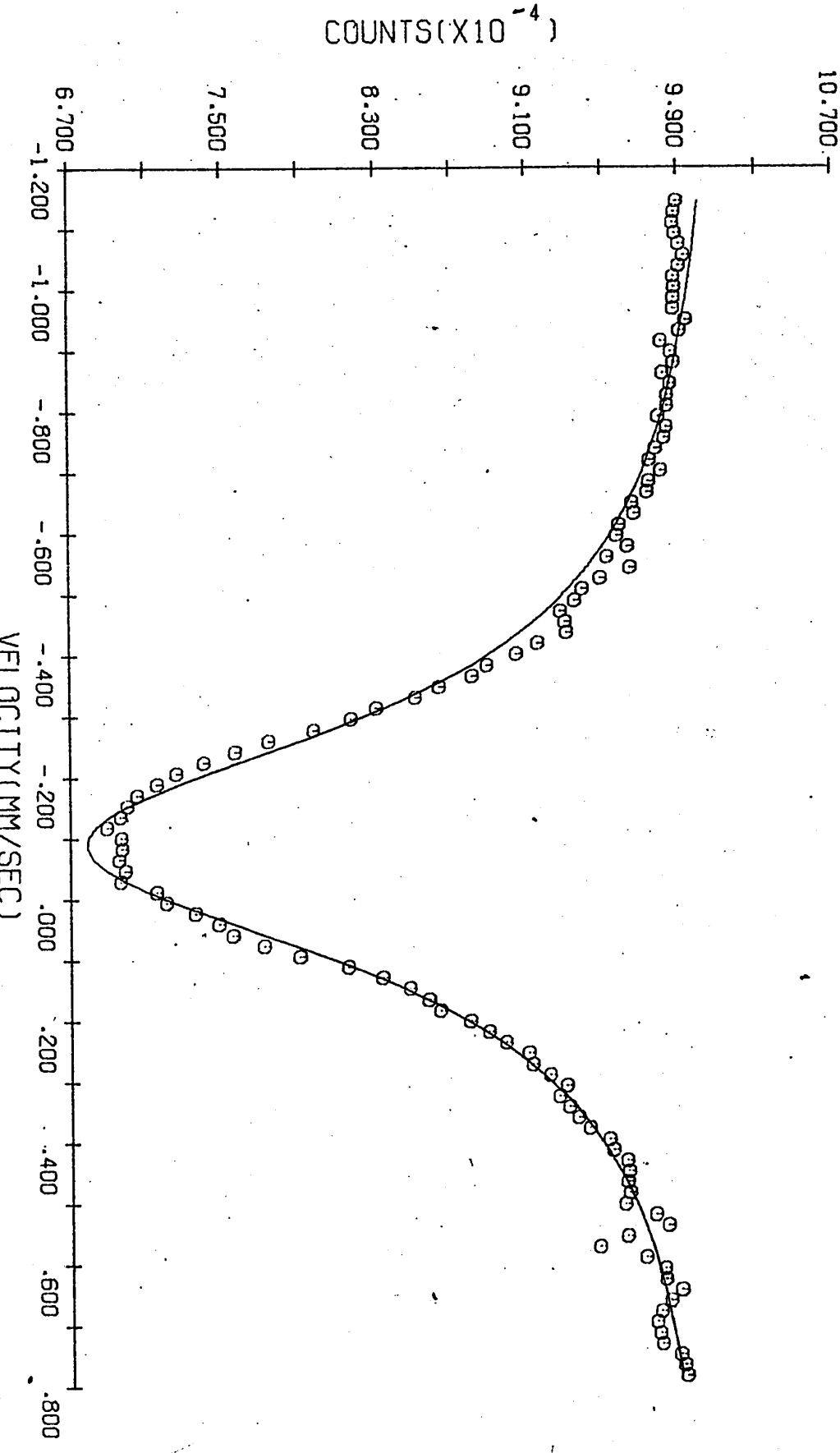

Fig.9b. MÖSSBAUER SPECTRUM OF STAINLESS STEEL

For source and absorber with different chemical environments, the difference in gamma ray energies is given by

$$\delta = E_{abs} - E_{source} = \frac{2}{5}\pi Ze^2\left[\langle r_b^2\rangle - \langle r_A^2\rangle\right]\left\{|\psi(0)|_a^2 - |\psi(0)|_s^2\right\}$$

$$= \frac{4\pi}{5} Ze^2 R^2 \left(\frac{\Delta R}{R}\right)\left\{|\psi(0)|_a^2 - |\psi(0)|_s^2\right\}$$

$$= 3.52 \times 10^9 \; R^2\left(\frac{\Delta R}{R}\right)\left\{|\psi(0)|_a^2 - |\psi(0)|_s^2\right\} \qquad (16)$$

where $\Delta R = R_{exc} - R_g$ with R_{exc}, R_g respectively the radii of the nuclei in the excited state and the ground state. Here R^2 and $|\psi(0)|^2$ are expressed in atomic units.

The isomer shift δ measured experimentally is thus only the product of a nuclear and an electronic term. There is no experimental technique at present which can measure either factor individually.

Walker et al. found from their measurements for Fe^{57} (18) :

$$\frac{\Delta R}{R} = -1.8 \times 10^{-3}$$

One can use this value and equation (15) to deduce the electron density at the nucleus for any other state of the iron atom for which the isomer shift has been measured.

The above result of $\frac{\Delta R}{R}$ is based on the assumption that the iron atom is completely ionized in its di- and trivalent states; but according to the Pauling principle of electroneutrality (19), the di- and trivalent ions are not in pure $3d^6$ or $3d^5$ states but $3d^5 4s^x$ and $3d^6 4s^x$, where x may be non integer. Once the $|\Psi(0)|^2$ are computed with the Hartree-Fock method and Fermi-Segrè formula for $3d^5$, $3d^6$, $3d^5 4s$ and $3d^6 4s$ (Table I), the value of x can be obtained from the measured isomer shift using a linear interpolation (Fig.11).

For instance, with the iron metal($3d^{8-x} 4s^x$), it has been found that $x = 1$. Nevertheless, for a more accurate treatment of the isomer shift, one should take into account not only the charge carried by the atom, but also the lattice forces and the covalent nature of the bond which distort the orbitals and thus influence the electron density at the nucleus. The problem has been approached in different ways and the difficulties are manifest through the range of different results given in Table II.

In order to use Fig.11 to deduce the electronic density $|\Psi(0)|^2$ of the iron compounds under investigation from the measured isomer shifts, it is necessary to calibrate the s-electron density scale in terms of these isomer shifts.

		$3d^8$	$3d^7$	Free ferrous ion $3d^6$	Free ferric ion $3d^5$	Free atom $3d^6 4s^2$
$\lvert\psi(0)\rvert^2$	1s	5,378.005	5,377.973	5,377.840	5,377.625	5,377.873
	2s	493.953	493.873	493.796	493.793	493.968
	3s	67.524	67.764	68.274	69.433	68.028
	4s					3.042
$\frac{\rho(0)}{4\pi}$		11,878.9	11,879.2	11,879.8	11,881.7	11,885.8

Table I. Electron density at r=0 for various configurations of the Fe atom

($\rho(0)$ is in atomic units : electrons per cubic Bohr radius)

$$\frac{\rho(0)}{4\pi} = 2 \sum_n |\psi_{ns}(0)|^2$$

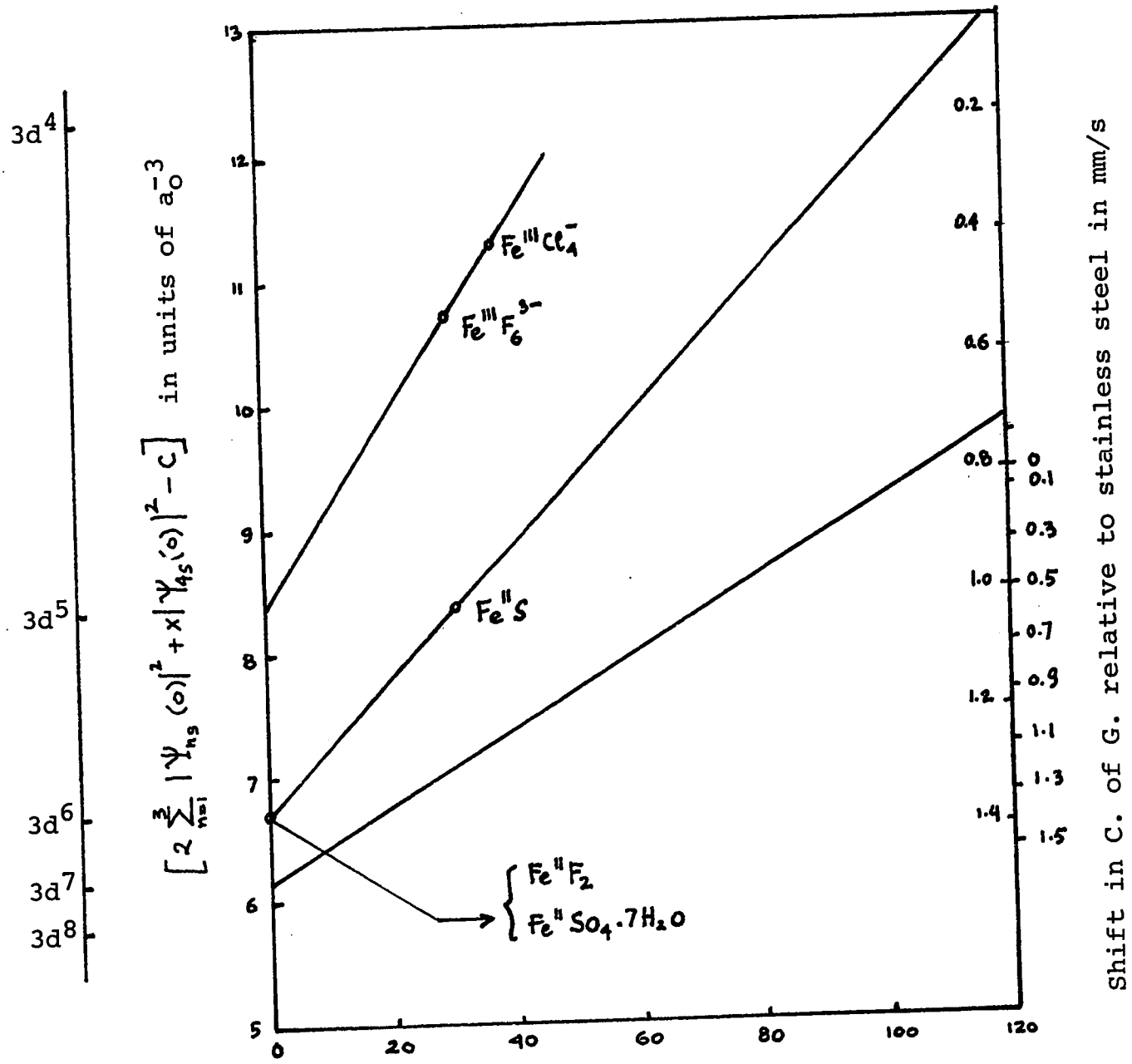

Fig.11. Total s-electron density as a function of the percentage of 4s character for various d-electron configurations. The outer scale on the right is from Walker et al.(18) and the inner scale is from Danon (22). (C= 11873 a_o^{-3})

Authors	Ref.	Value of $\frac{\Delta R}{R}$ for Fe^{57}
Walker et al.	(18)	-1.8×10^{-4}
Wegener	(20)	-1.2×10^{-4}
Goldanski	(21)	-0.5×10^{-4}
Danon	(22)	-1.1×10^{-4}
Goldanski et al.	(23)	-0.9×10^{-3}
Šimaneck et al.	(24)	$-4.$ to -5.2×10^{-4}

Table I. Relative change of radius of the Fe^{57} nucleus between the first excited and ground states.

Table III summarizes the isomer shifts of various iron compounds at room temperature relative to a Co^{57} stainless steel source.

	Fe^{2+}	Fe^{3+}	Fe(II) cov.	Fe(III) cov.
Danon (22)	~ 1.4	~ 0.5	~ 0.1	~ 0mm/s
Duncan (25)	1.0 to 1.5	0.3 to 1.0	0.2 to 0.3	0.4 to 0.5mm/s

Table III. Isomer shifts of various iron compounds

The electron densities at the nucleus have been found in the order (22) :

$$|\Psi(0)|^2_{2+} < |\Psi(0)|^2_{3+} < |\Psi(0)|^2_{\text{II cov.}} < |\Psi(0)|^2_{\text{III cov.}} \quad (17)$$

3.3 Magnetic splitting

The Hamiltonian of the interaction of the nuclear magnetic dipole moment $\vec{\mu}$ with a magnetic field $\vec{H}$ is given by

$$\mathcal{H}_M = -\vec{\mu}.\vec{H} = -g_n \mu_n \vec{I}.\vec{H} \tag{18}$$

where $\vec{I}$ is the nuclear spin, g_n the nuclear splitting factor, and μ_n the nuclear magneton. The energy level is split into $2I + 1$ components with energies :

$$E_\mu = - g_n \mu_n m H \tag{19}$$

where $m = I, I-1, \ldots, -I$. The splittings can be observed only when

$$\Delta E_\mu = \left| \frac{\mu H}{I} \right| > 2\Gamma \tag{20}$$

Figures 12 and 13 show respectively the Mössbauer spectrum of natural iron and the corresponding allowed magnetic dipole transitions ($\Delta m = 0, \pm 1$) between the $3/2^-$ and $1/2^-$ states. The relative position of the lines depends on the ratio of the magnetic moments of Fe^{57} in the ground state and in the excited state. Measurements from the spectrum give the following results (26) for the $3/2^-$ state:

$$\mu = -0.153 \text{ nm} \pm 0.004$$
$$H = -333 \text{ kOe} \pm 10 \text{ at room temperature}$$

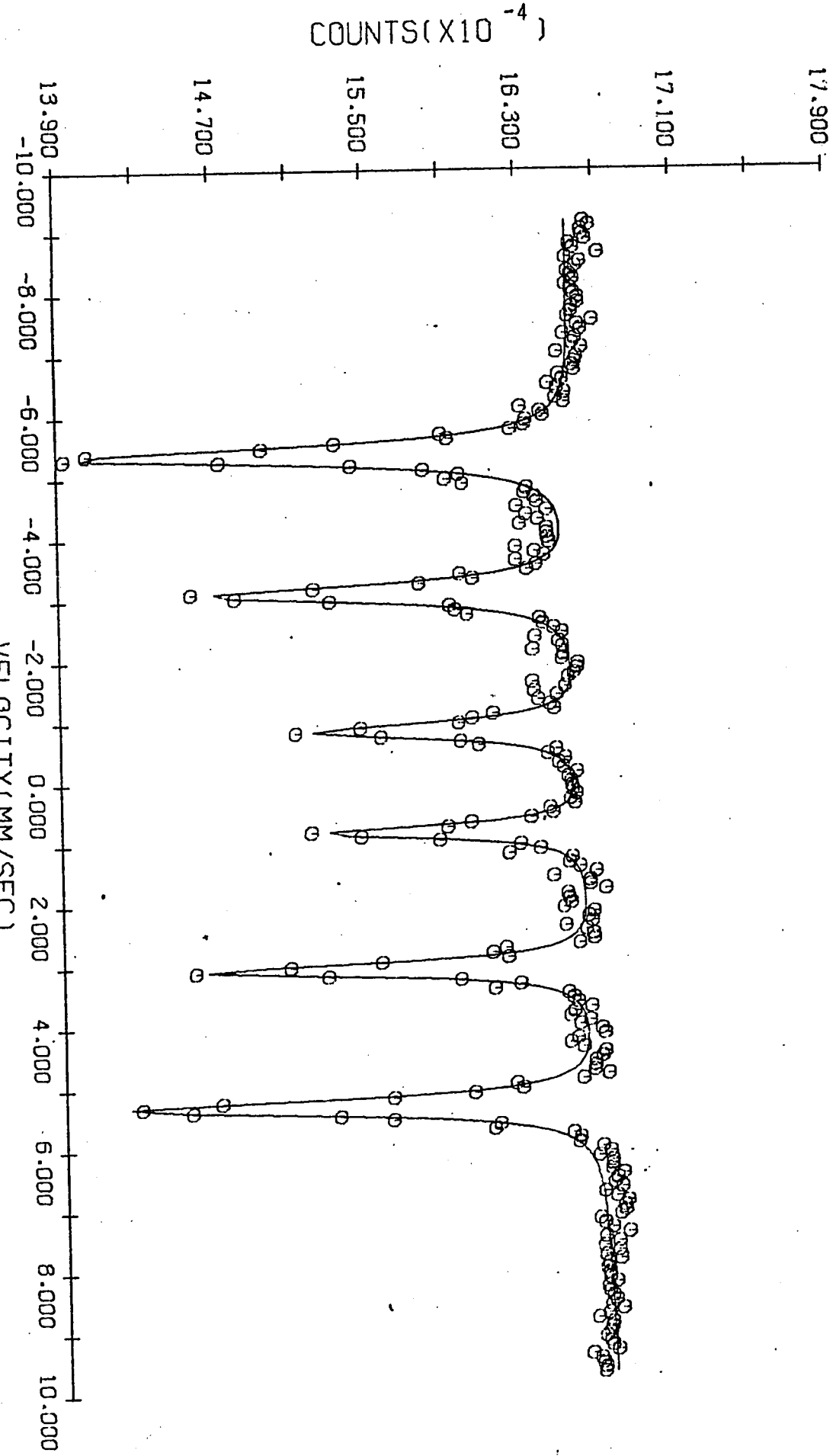

Fig 12.. MÖSSBAUER SPECTRUM OF NATURAL IRON

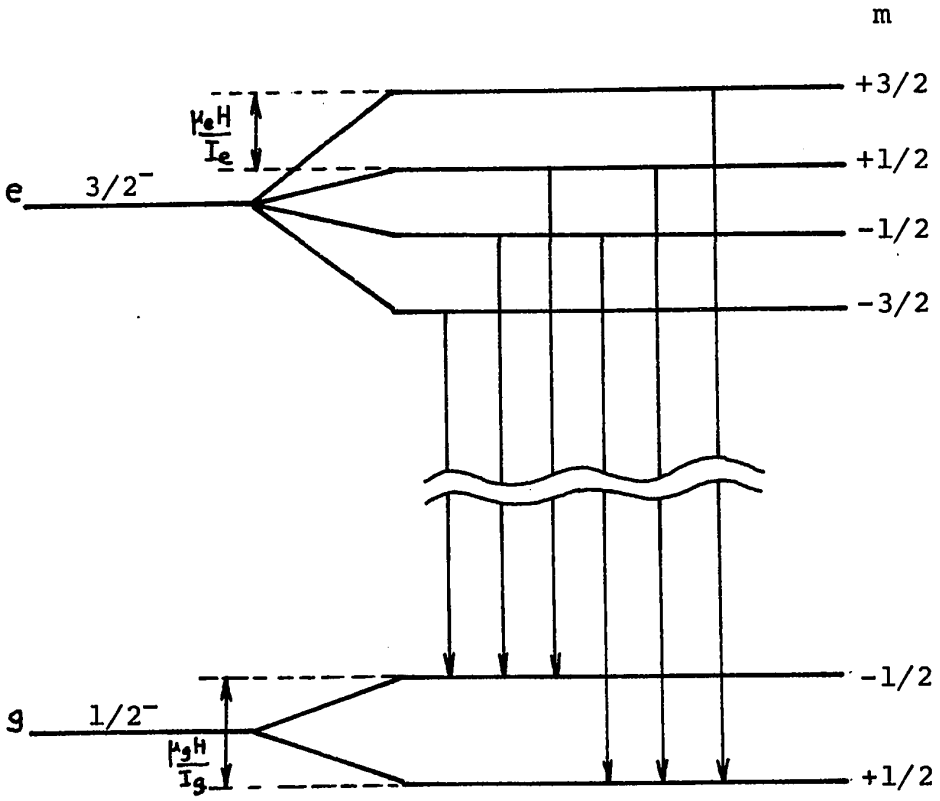

Fig.13. Magnetic hyperfine splittings of the first excited and ground states of Fe^{57}.

The sign of the internal field at the nucleus is determined by observing the direction of the shift of the lines caused by an applied external field. The negative sign, due to the core polarization, means that the direction of the field is antiparallel to the direction of magnetization.

The above results may be explained by making use of the Hamiltonian of a Dirac electron in the Coulomb field of the nucleus (27) :

$$\mathcal{H}_M = -2\mu_B \left\{ \frac{\vec{L}-\vec{S}}{r^3} + \frac{3(\vec{S}.\vec{r})\vec{r}}{r^5} + \frac{8\pi}{3}\delta(\vec{r})\vec{S} \right\} \vec{\mu} \qquad (21)$$

where μ_B is the Bohr magneton and $\vec{L}$ and $\vec{S}$ are the orbital angular momentum and spin of the electron. The vector operator

$$2\mu_B \left\{ \frac{\vec{L}-\vec{S}}{r^3} + \frac{3(\vec{S}.\vec{r})\vec{r}}{r^5} + \frac{8\pi}{3}\delta(\vec{r})\vec{S} \right\} \qquad (22)$$

may be interpreted as an effective field produced by the electrons at the nucleus. The two first terms are similar to those for electrostatic dipole interaction and the last term is the Fermi contact term, derived from the Dirac equation, which has a δ-dependence at the nucleus.

Using $$E_\mu = \int \Psi^* \mathcal{H}_M \Psi \, d\tau \qquad (23)$$

One obtains from equations (18)(21)and (23)

$$\vec{H} = -\frac{8\pi}{3}\mu_B |\psi_\uparrow(0)|^2 \vec{S} - 2\mu_B \langle \frac{1}{r^3} \rangle \langle \vec{L} \rangle - \frac{2\mu_B}{r^5} \langle 3(\vec{r}\cdot\vec{S})\vec{r} - r^2\vec{S} \rangle \quad (24)$$

where $|\psi_\uparrow(0)|^2$ is the electron density at the nucleus with $+\frac{1}{2}$ spin projection. The first term, coming from the Fermi contact interaction, gives the largest contribution to the magnitude of the internal field.It is the spin interaction between the nuclear and electron spins, and has a value of -300 kOe according to a theoretical calculation of Watson and Freeman (28). The second term, which is the interaction of the nucleus with the electron orbital magnetic moment, contributes to the internal field only for non s-state ions. The last term is the nuclear dipole interaction with the moment of the electron spin; it is of the order of +100 kOe and zero for cubic symmetry ions.

The dipolar and Fermi contact terms are both dependent on the orientation of the net electron spin $\vec{S}$ which is related to the electron spin lattice relaxation time. Therefore, hyperfine structure is present only when the frequency of the electron spin "flips" is of the order of or smaller than the Larmor frequency of the nuclear spin.

3.4. Quadrupole splitting

The interaction of the electric field gradient (EFG) tensor, produced by the surrounding charges about the nucleus and the nuclear electric quadrupole moment eQ, is expressed in the first order by the Hamiltonian operator

$$\mathcal{H}_Q = \frac{e^2Qq}{4I(2I-1)}\left[3\hat{I}_z^2 - \hat{I}^2 + \frac{\eta}{2}(\hat{I}_+^2 - \hat{I}_-^2)\right] \qquad (25)$$

where $eq = V_{zz}$ is the EFG tensor along the z-axis at the nucleus, $\eta = \frac{V_{xx} - V_{yy}}{V_{zz}}$ is the asymetry parameter and $\hat{I}_\pm = \hat{I}_x \pm i\hat{I}_y$ are the raising and lowering operators.

Defining

$$A = \frac{e^2Qq}{4I(2I-1)} \qquad (26)$$

equation (25) becomes

$$\mathcal{H}_Q = A\left[3\hat{I}_z^2 - \hat{I}^2 + \frac{\eta}{2}(\hat{I}_+^2 - \hat{I}_-^2)\right] \qquad (27)$$

In order to calculate the elements of the Hamiltonian matrix, we make use of the following expressions :

$$\begin{aligned}
\langle I_{m\pm1}|\hat{I}_\pm|I'_{m'}\rangle &= \sqrt{(I\mp m')(I\pm m'+1)}\;\delta_{II'}\,\delta_{m\,m'\pm1} \\
\langle I_m|\hat{I}^2|I'_{m'}\rangle &= I(I+1)\,\delta_{II'}\,\delta_{mm'} \\
\langle I_m|\hat{I}_z|I'_{m'}\rangle &= m\,\delta_{II'}\,\delta_{mm'}
\end{aligned} \qquad (28)$$

Thus :

$$\left\langle \tfrac{3}{2}m\middle|\mathcal{H}_Q\middle|\tfrac{3}{2}m'\right\rangle = \begin{array}{c} \\ m' \\ 3/2 \\ 1/2 \\ -1/2 \\ -3/2 \end{array} \begin{array}{c} \begin{array}{cccc} m & 3/2 & 1/2 & -1/2 & 3/2 \end{array} \\ \begin{bmatrix} 3A & 0 & \sqrt{3}\eta A & 0 \\ 0 & -3A & 0 & \sqrt{3}\eta A \\ \sqrt{3}\eta A & 0 & -3A & 0 \\ 0 & \sqrt{3}\eta A & 0 & 3A \end{bmatrix} \end{array} \qquad (29)$$

The off-diagonal terms are introduced by the raising and lowering operators. The eigenvalues and their corresponding eigenvectors are respectively (29) :

$$
\begin{aligned}
E_+ &= +3A\left[1 + \eta^2/3\right]^{1/2} \qquad |+\rangle = N_+\left(\lambda_+ \left|\tfrac{3}{2},\tfrac{3}{2}\right\rangle + \left|\tfrac{3}{2},-\tfrac{1}{2}\right\rangle\right) \\
E_- &= -3A\left[1 + \eta^2/3\right]^{1/2} \qquad |-\rangle = N_-\left(\lambda_- \left|\tfrac{3}{2},\tfrac{3}{2}\right\rangle + \left|\tfrac{3}{2},-\tfrac{1}{2}\right\rangle\right) \\
E_- &= -3A\left[1 + \eta^2/3\right]^{1/2} \qquad |-\rangle' = N_-\left(\lambda_- \left|\tfrac{3}{2},-\tfrac{3}{2}\right\rangle + \left|\tfrac{3}{2},\tfrac{1}{2}\right\rangle\right) \\
E_+ &= +3A\left[1 + \eta^2/3\right]^{1/2} \qquad |+\rangle' = N_+\left(\lambda_+ \left|\tfrac{3}{2},-\tfrac{3}{2}\right\rangle + \left|\tfrac{3}{2},\tfrac{1}{2}\right\rangle\right)
\end{aligned}
\tag{30}
$$

where

$$N_\pm = \left[1 + \lambda_\pm^2\right]^{-1/2} \tag{31}$$

$$\lambda_\pm = \frac{\sqrt{3}}{\eta}\left(1 \pm \sqrt{1+\eta^2/3}\right) \tag{32}$$

For Fe^{57}, eQ is positive and the coefficient A carries the sign of V_{zz}. Figures (14a) (14b) show respectively the two cases where $\eta = 0$ and $\eta \neq 0$.

In the case of combined magnetic and quadrupole interactions, three simple cases can be considered (27) :

(i) $\eta = 0$, the EFG has axial symmetry around the z-axis with $\vec{H}$ parallel to the symmetry axis :

$$E = -g_n \mu_n H + (-1)^{|m|+\frac{1}{2}} e^2 q Q/4 \tag{33}$$

(ii) $\eta \neq 0$ with $\vec{H}$ parallel to one of the principal axes

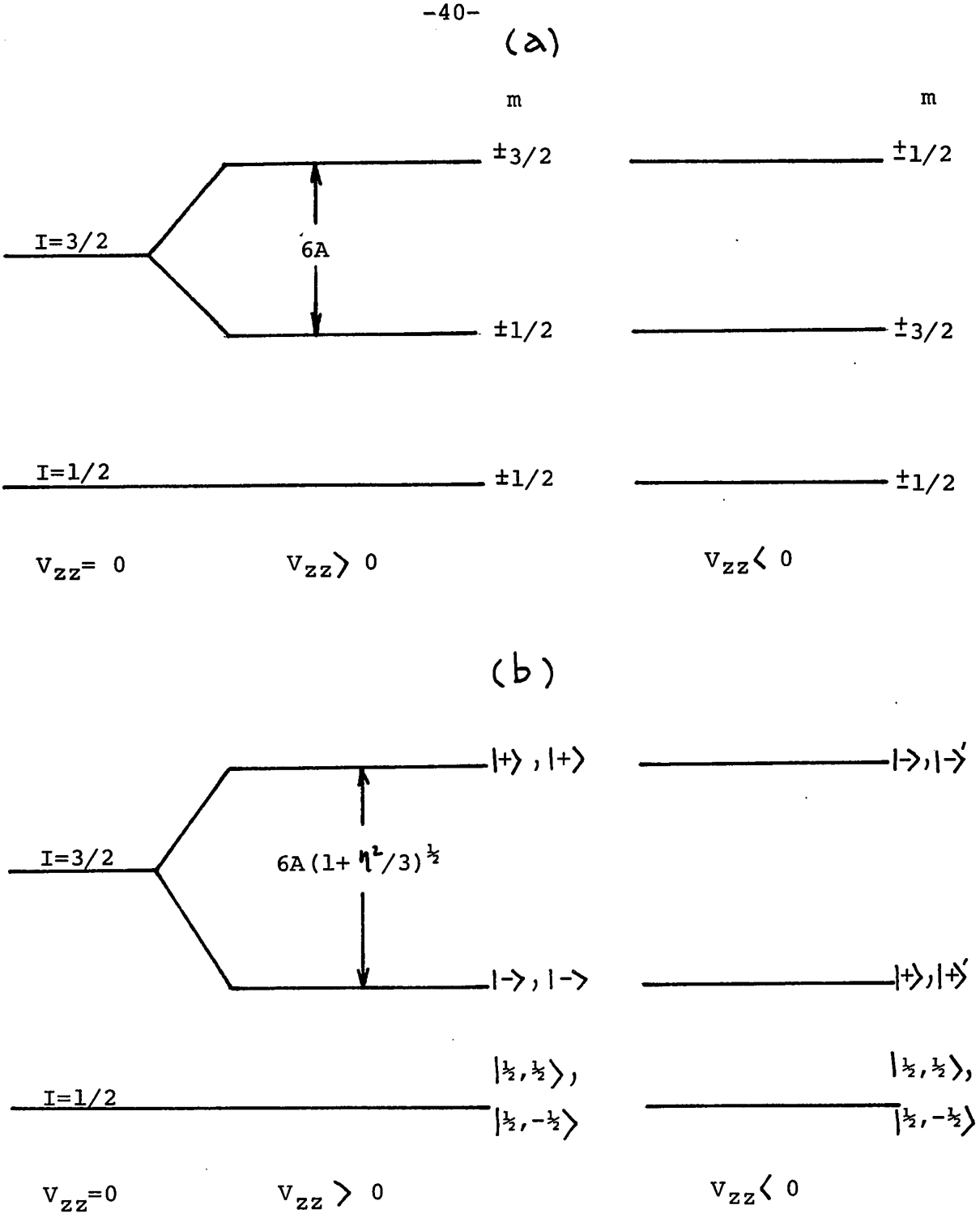

Fig. 14. Quadrupole splitting of the $3/2^-$ state of Fe^{57}.

of V_{ij} :

$$E = \begin{cases} \frac{1}{2} g_n \mu_n H \pm \frac{1}{4} e^2 q Q \left[\left(1 + \frac{4 g_n \mu_n H}{e^2 q Q}\right)^2 + \frac{1}{3}\eta^2 \right]^{1/2} \\ -\frac{1}{2} g_n \mu_n H \pm \frac{1}{4} e^2 q Q \left[\left(1 - \frac{4 g_n \mu_n H}{e^2 q Q}\right)^2 + \frac{1}{3}\eta^2 \right]^{1/2} \end{cases} \quad (34)$$

(iii) $\eta = 0$ with $\vec{H}$ making an arbitrary angle θ with the symmetry axis of V_{ij}; there is no closed formulae, only machine calculations are available (30).

Neither formulae nor calculations are available for the general case of arbitrary η and θ. A general quantitative treatment of the quadrupole interaction is very difficult and is still open to discussion. Some qualitative ideas will be reported in the next chapter in some particular cases of our studies.

CHAPTER IV

INTERPRETATION OF THE MÖSSBAUER SPECTRA

4.1. Atomic properties of Iron

The iron atom has 26 electrons, the first 18 electrons form an inert Argon core and the 8 remaining electrons belong to the 3d and 4s shells :

$$1s^2 2s^2 2p^6 3s^2 3p^6 3d^6 4s^2$$

The 4s shell is filled and represents a spherically symmetric distribution. The 3d states with $\ell = 2$ are quintuply degenerate and the angular dependence of the states is expressed by five spherical harmonics Y_ℓ^m ($m=-2,-1,0,1,2$). In order to study how the degeneracy is removed by a crystal field, it is convenient to combine these spherical harmonics into a set of degenerate states having simple symmetry properties upon inversion of each axis (octahedral or tetragonal symmetry) (31) :

$$\begin{aligned} Y_2^{(1+)} &\equiv |yz\rangle = \frac{i}{\sqrt{2}}\left(Y_2^1 + Y_2^{-1}\right) = \sqrt{\frac{15}{4\pi}}\ \frac{yz}{r^2} \\ Y_2^{(1-)} &\equiv |xz\rangle = -\frac{1}{\sqrt{2}}\left(Y_2^1 - Y_2^{-1}\right) = \sqrt{\frac{15}{4\pi}}\ \frac{xz}{r^2} \\ Y_2^{(2-)} &\equiv |xy\rangle = \frac{1}{i\sqrt{2}}\left(Y_2^1 - Y_2^{-2}\right) = \sqrt{\frac{15}{4\pi}}\ \frac{xy}{r^2} \end{aligned} \qquad (35)$$

$$Y_2^{(2+)} \equiv |x^2-y^2\rangle = \frac{1}{\sqrt{2}}\left(Y_2^2 + Y_2^{-2}\right) = \sqrt{\frac{15}{16\pi}}\ \frac{x^2-y^2}{r^2}$$

$$Y_2^{(0)} \equiv |3z^2-r^2\rangle = Y_2^0 = \sqrt{\frac{5}{16\pi}}\left(\frac{3z^2-r^2}{r^2}\right)$$

The first three states denoted by d_ϵ are called triplet states and the last two denoted by d_γ are called doublet states. Their graphical representations are shown in Figure 15. In a cubic field, where the positive ion is surrounded by six equidistant negative ions located at the vertices of a regular octahedron, the free ion state is split into d_γ and d_ϵ states. The d_ϵ states lie lower since their wave functions do not point toward the negative charges; therefore, the electrostatic repulsion is smaller (Figure 15). The degeneracy of the d_ϵ and d_γ states will be completely removed by appropriate fields as shown in Figure 16.

Most iron ions are either ferric Fe^{3+} or ferrous Fe^{2+}. They are distributed into two different electronic configurations called high- and low-spin compounds as shown in Figure 17.

The magnetic moment can be calculated from the number n of unpaired electrons by the expression:

$$\mu_{spin} \simeq \left[n(n+2)\right]^{1/2} \quad \text{Bohr magnetons} \qquad (36)$$

From Figure 17, one can see that in high-spin

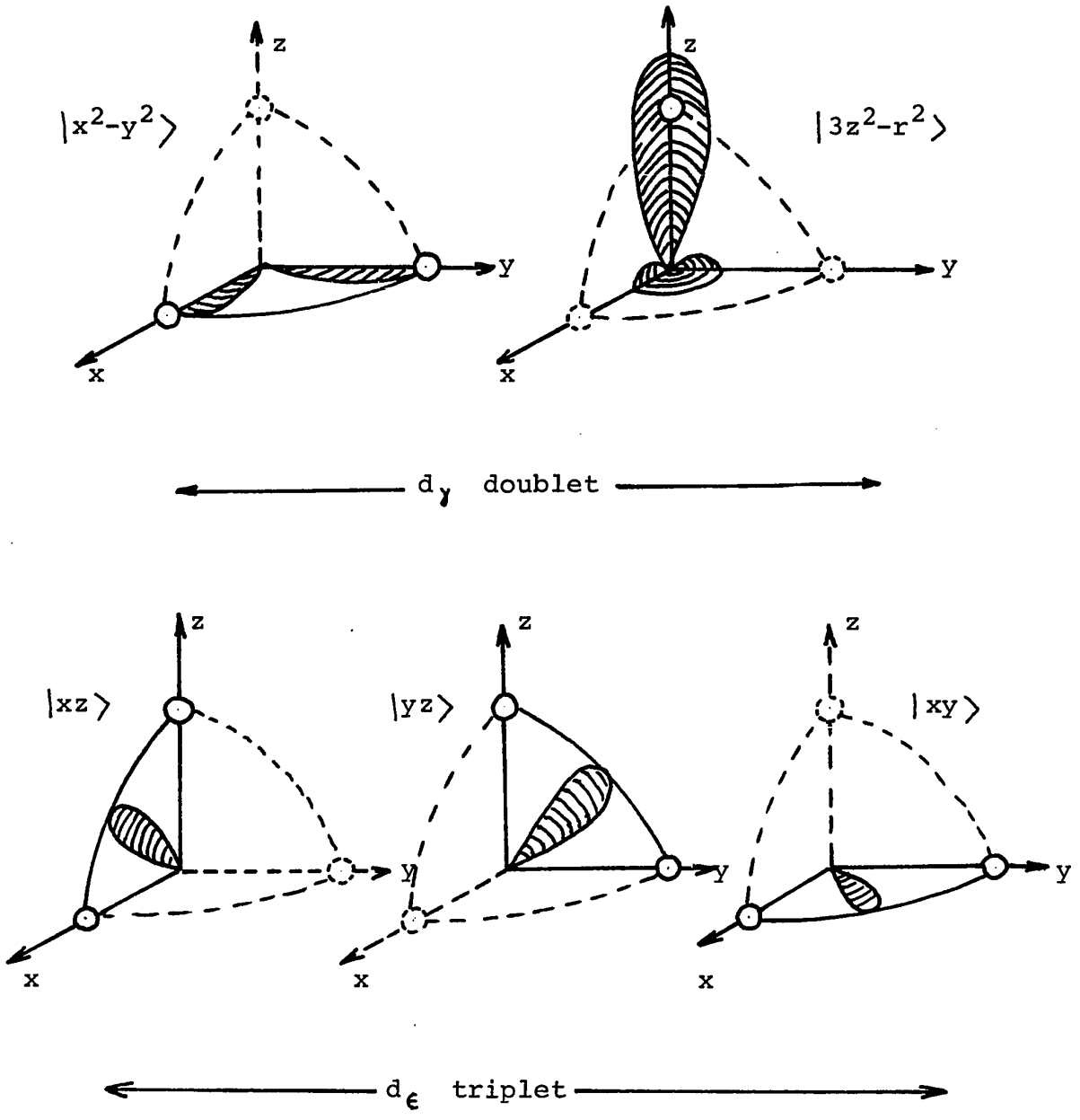

Fig.15. Polar plot of the functions $Y_2^{m\pm}$ in the first quadrant. Small circle represent negative charges.

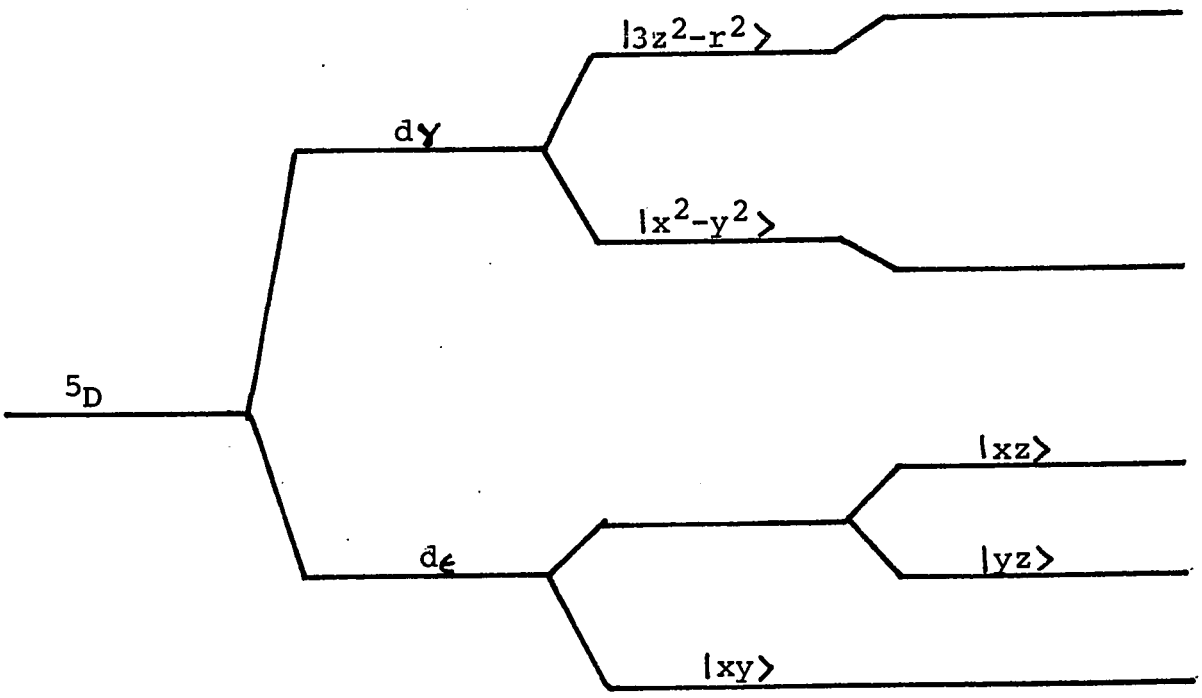

Fig. 16. Schematic representation of the splittings of the d orbitals in a transition metal by a crystalline electric field.

IRON III, $3d^5$				IRON II, $3d^6$			
High-spin		Low-spin		High-spin		Low-spin	
d^3d^2 , $^6S_{5/2}$		d^5 , ^2D		d^4d^2 , $^5D_4$		d^6 , $^1S_0$	
(Fe^{3+})		(covalent)		(Fe^{2+})		(covalent)	
d_ϵ	d_γ	d_ϵ	d_γ	d_ϵ	d_γ	d_ϵ	d_γ
↑ ↑ ↑	↑ ↑	↑↓ ↑↓ ↑		↑↓ ↑ ↑	↑ ↑	↑↓ ↑↓ ↑↓	
5.92		1.73	μ_{spin}	4.90		0	

Fig.17. Diagram showing the occupation of the d orbitals, the spins and magnetic moments of iron ions.

ferric salt, the charge distribution is spherically symmetrical; thus does not contribute to the EFG at the nucleus. The lattice effects are the only responsible factors for any existing quadrupole splitting. In high-spin ferrous iron ($\ell = 2$), Fe^{2+} has a Fe^{3+} spherically symmetric core with one additional d-electron. In this case, the ion affects the quadrupole splitting. Table IV shows the substantial difference in the quadrupole splittings between high-spin compounds of the two oxidation states of iron. For low-spin ions, the nature of the bonding to ligands is strongly involved. The repulsion between the 3d electrons is overcome by the crystal forces and the Hund's rule is no more applicable. This situation is typical of complexes with paired spins. In particular, the low-spin ferrous ion, where all the $6d_\epsilon$ states are filled, exhibits a cubic symmetry and is diamagnetic.

	Fe^{2+}	Fe^{3+}	
ΔE	0.15 to 0.37	0.0 to 0.1	cm/s

Table IV. Typical magnitudes of the quadrupole splittings (ΔE) in high-spin iron compounds

4.2. Computation and Results

The peaks of natural iron are used to calibrate the velocity spectrometer. Taking the values for g_1 and g_o of the hyperfine splittings of the first excited and the ground states of Fe respectively as (26):

$$g_1 = 2.23 \pm 0.03 \text{ mm/s.}$$
$$g_o = 3.96 \pm 0.10 \text{ mm/s.}$$

The velocities corresponding to the six peaks of the iron spectrum are found to have the following values :

$$\pm 0.865, \quad \pm 3.095 \quad \text{and} \quad \pm 5.325 \text{ mm/s.}$$

For each range of maximum velocity, attained by the transducer, the positions of the peaks are determined experimentally. The above velocities are assigned to them according to their positions. A least-squares fitting is then made with a computer. Assuming a linear dependence of the positions with regard to the velocity, a calibration equation is found which serves to compute the velocities of the absorption peaks of the unknown spectra. Table V summarizes the results obtained for the iron halide complexes, the ferrocene acetonitrile and its titanium derivative. The isomer shifts refer to the sodium

nitroprusside as a standard, the shift for which is -0.483mm/s relative to a Co^{57} source embedded in copper (32).

Compound	Isomer shift (mm/s)	Quadrupole splitting (mm/s)
$FeCl_2.2HCONH_2$	1.85	2.30
$FeCl_2.2HCONHCH_3$	1.94	2.37
$Fe(CH)_9CCH_2CN$	0.87	2.28
$Fe(CH)_9CCH_2CNTiCl_4$	0.91	----

Table V. Isomer shifts and quadrupole splittings of some iron salts (see Fig.18,19,20 and 21).

These results when compared to those given in Table III and Table IV suggest strongly that the iron halide complexes belong to the high-spin ferrous group. The free ion Fe^{2+} state is $^5D_4$ (Fig.17). Its total angular momentum is $\vec{J}=4$ resulting from the spin-orbit coupling which favors parallel $\vec{L}$ and $\vec{S}$ when the shell is more than half-full. The high-spin ferrous salt Fe^{2+} have an odd d-electron outside the spherically symmetrical half filled 3d-shell, its spin is antiparallel to those of the other five electrons. If the Jahn-Teller effect is neglected, the splitting occurs only if the iron is in a lattice whose symmetry is lower than cubic. This confirms the tetrahedral configuration suggested previously by Singh and

Rivest(5). The EFG in a ferrous compound is given by(33)

$$q_{Fe^{2+}} = (1-R)\,q_{val} + (1-\gamma_\infty)\,q_{lat} \qquad (37)$$

and correspondingly

$$\eta\, q_{Fe^{2+}} = (1-R)\,q_{val}\,\eta_{val} + (1-\gamma_\infty)\,q_{lat}\,\eta_{lat} \qquad (38)$$

where the indexes *lat* and *val* refer to the contributions of the lattice and the odd d-electron, $(1-R)$ and $(1-\gamma_\infty)$ are the Sternheimer factors which correct for the polarization of the ferric core by the EFG of the odd electron and lattice charge distributions. In a first approximation, q_{lat} can be neglected and one writes :

$$q_{Fe^{2+}} \cong (1-R)\,q_{val} \qquad (39)$$

For a free ion, and neglecting the spin-orbit interaction (34) :

$$q_{Fe^{2+}} = 0.68 \times \frac{4}{7} \langle r^{-3} \rangle_{3d} = 0.3885 \langle r^{-3} \rangle_{3d} \qquad (40)$$

Theoretical calculations from Freeman and Watson(35) yield a value of $\langle r^{-3} \rangle_{3d} = 4.8$ a.u..Taking into account the effects of covalency, spin-orbit coupling and the crystalline EFG Ingalls(33) derives a value of $+0.29 \pm 0.02$ barns for the quadrupole moment of Fe^{57m}. The experiment was carried out at low temperature so that the odd d-electron will be localized in the ground state d-orbital.

The relatively small values of the isomer

shifts of the second set of results suggest that the ferrocene acetonitrile and its titanium derivative are either low-spin ferrous or ferric compounds. Nevertheless, the order of magnitude of the quadrupole splitting of ferrocene acetonitrile indicates that they both belong rather to the low-spin ferrous group. In both cases, because of the small values of the isomer shifts, there is a strong 4s-covalent contribution. Since a low-spin ferrous compound possesses a cubic symmetry and thus should not contribute to the quadrupole splitting, the existence of a splitting in the ferrocene acetonitrile may arise from a strong distortion of the iron environment.

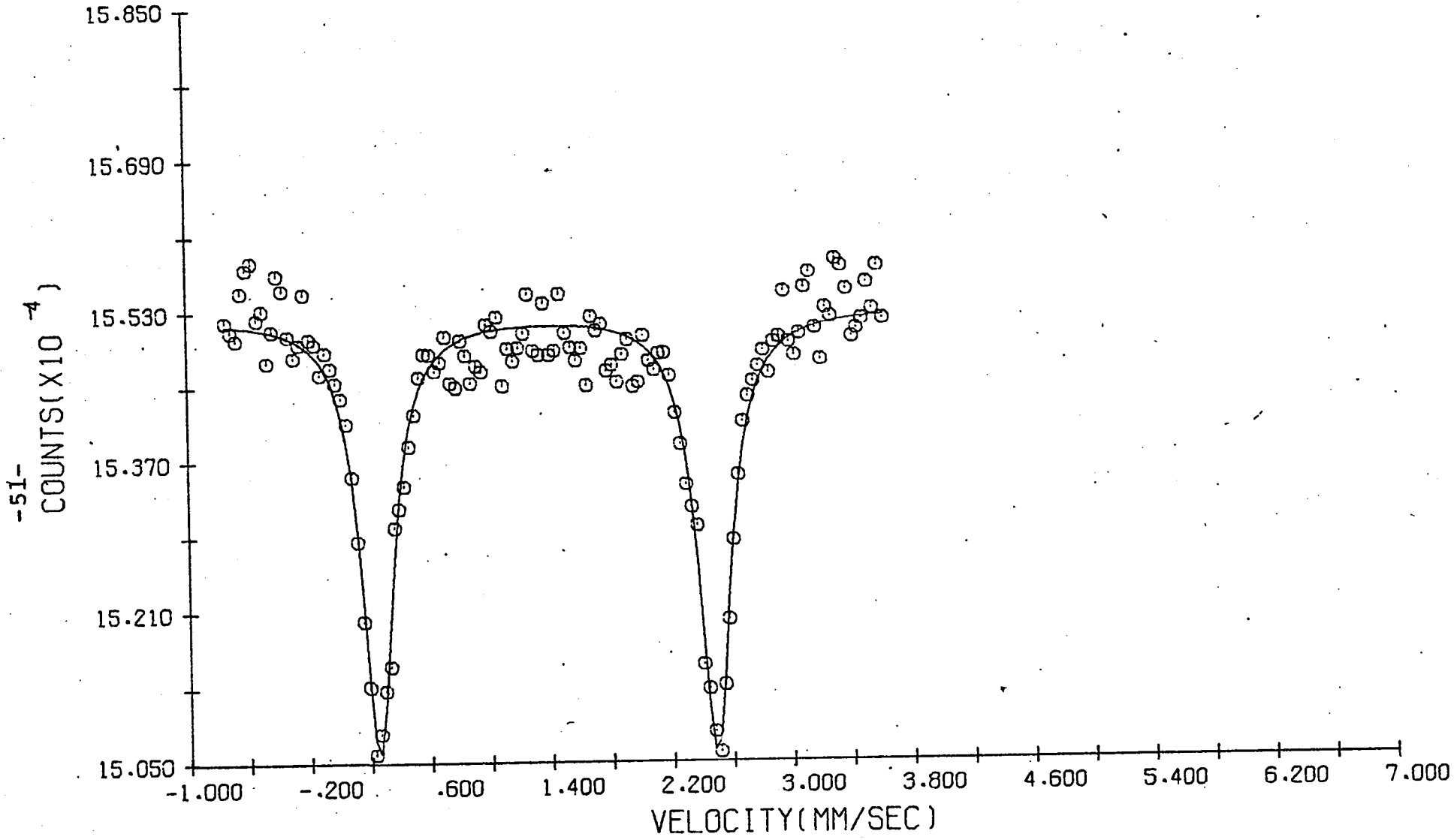

Fig.18. MÖSSBAUER SPECTRUM OF FECL2.2HCONH2

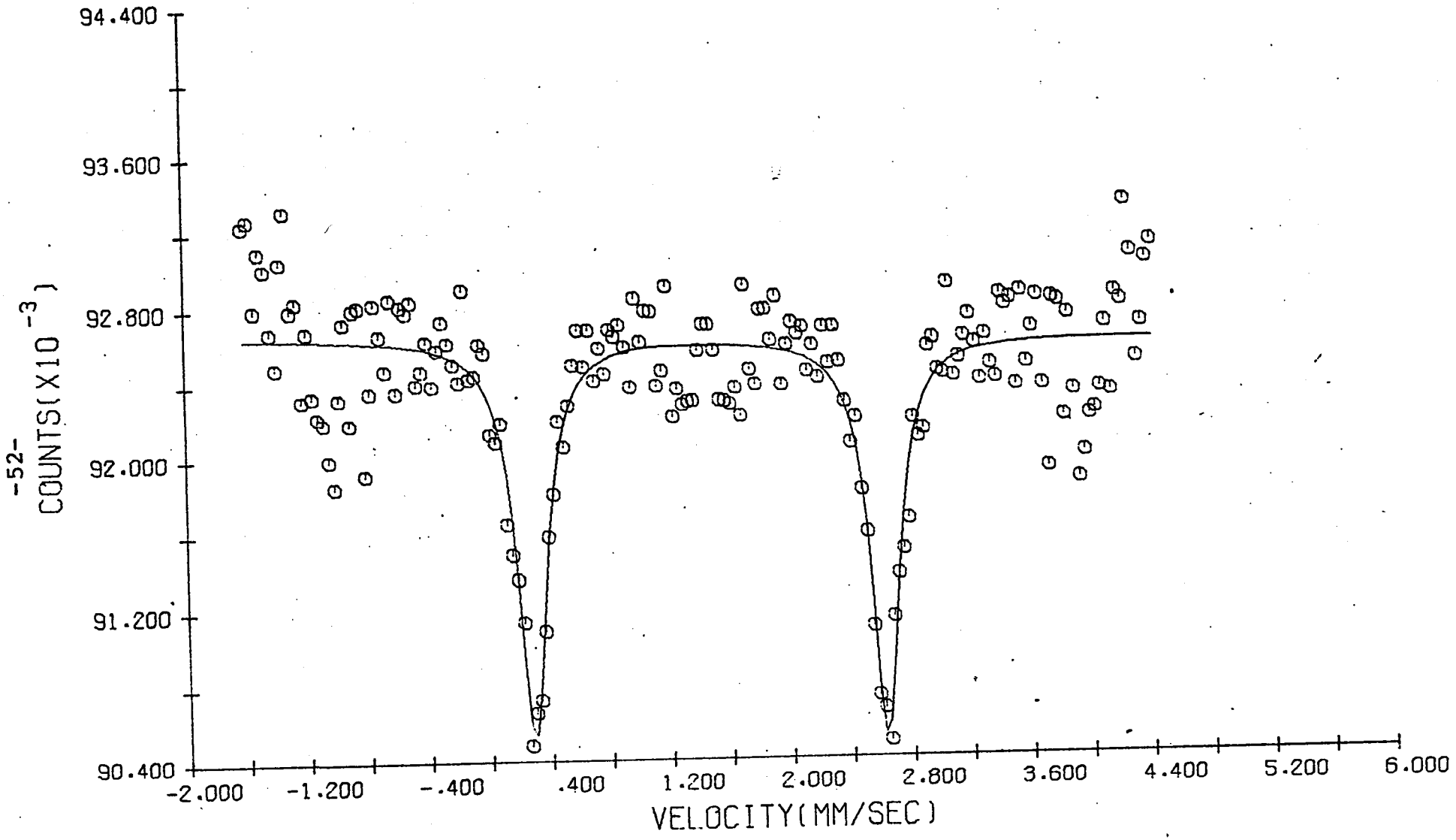

Fig. 19. MÖSSBAUER SPECTRUM OF FECL2.2HCONHCH3

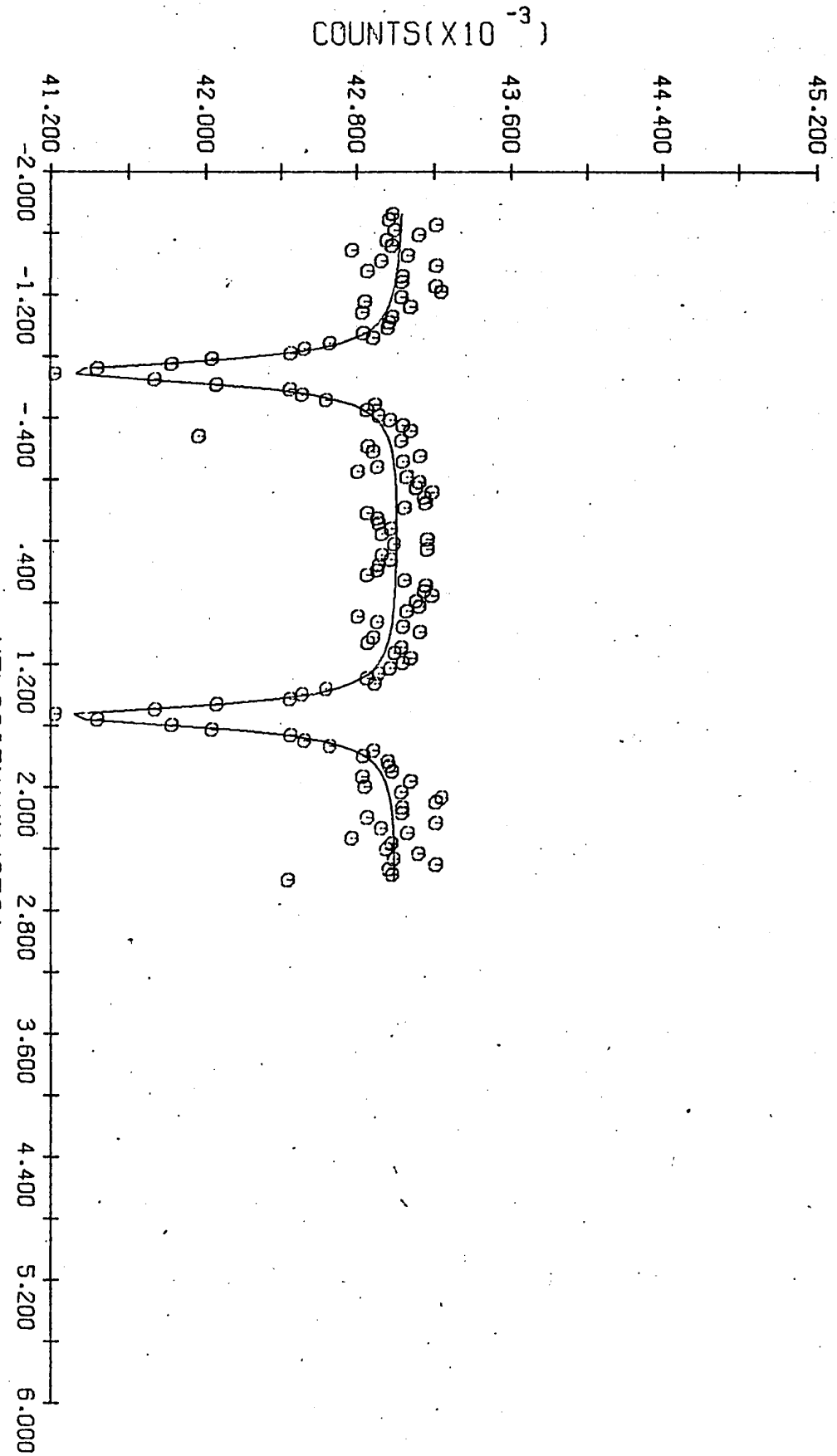

Fig.20. MÖSSBAUER SPECTRUM OF FE(CH)9CCH2CN

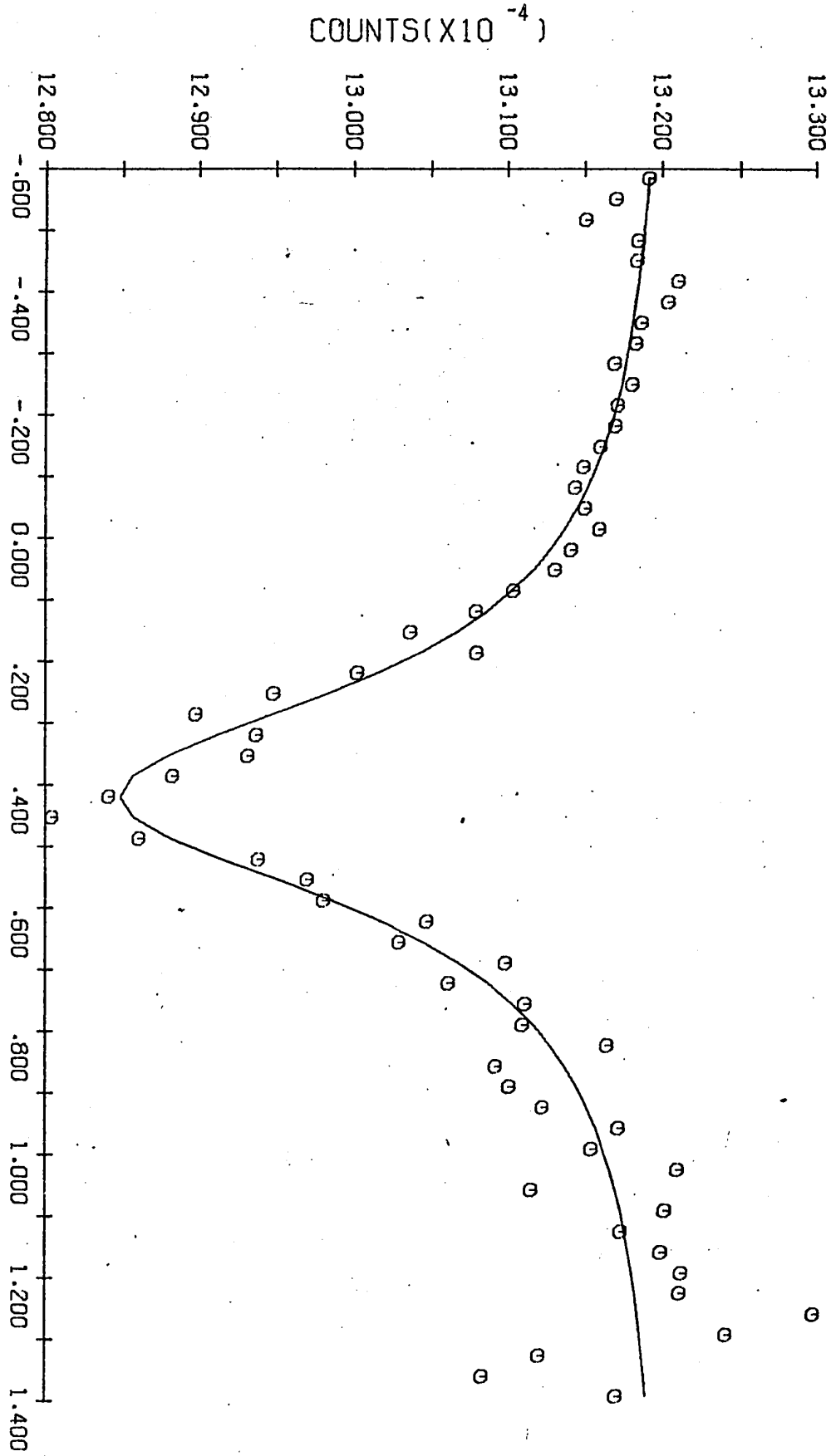

Fig.21. MÖSSBAUER SPECTRUM OF FE(CH)9CCH2CNTICL4

CHAPTER V

CONCLUSION

In studying the Mössbauer effect of some iron salts, we have reviewed the general aspects of this field of study; especially its applications and inherent problems the solutions of which would bring a more precise and quantitative interpretation of the experimental data.

The salts under investigation are all ferrous compounds, they are high-spin for the halide complexes which possibly possess a tetrahedral configuration, and low-spin for the ferrocene acetonitrile and its titanium derivative. Low temperature experiments would probably give more information about the nature of the ligand fields which are strongly involved in the second case.

A curve-fitting computer program, given in the Appendix, provides a fast and precise means to the study of the line shape, line width, line position and line area of the experimental Mössbauer spectra.

APPENDIX

LEAST-SQUARES CURVE FITTING

The best least-squares fitting occurs when there exist parameters p which can minimize the function defined by

$$\chi^2 = \sum_{i=1}^{N} \left(\frac{\theta_i^{exp} - \theta_i(\vec{p})}{\Delta\theta_i^{exp}} \right)^2 \qquad (1)$$

where θ_i^{exp} = measured number of counts in the ith channel, $\theta_i(\vec{p})$ = corresponding number of counts calculated from an approximate knowledge of the parameters and model and $\Delta\theta_i^{exp}$ = experimental error on θ_i^{exp}.

For a Lorentzian line shape :

$$\theta_i(\vec{p}) \equiv \theta_i(A_j, x_j, C_j) = B + \sum_{j=1}^{M} \frac{A_j}{1 + \left(\frac{x_i - x_j}{C_j}\right)^2} \qquad (2)$$

where B is the background, M the number of Lorentzian lines, A_j the line amplitude, C_j the half width at half maximum and x_i and x_j are the channel numbers.

The necessary condition for minimization of χ^2 is

$$\vec{\nabla}\chi^2 = 0 \quad \text{or} \quad \frac{\partial\chi^2}{\partial p_j} = 0 \quad \text{with} \quad j = 1, \ldots 3M \qquad (3)$$

It is sufficient if all the eigenvalues of the second derivative matrix are positive. Actually, condition(3) is

only satisfied to a certain degree i.e.

$$\Delta \chi^2 = \epsilon \tag{4}$$

where ϵ is a small number depending on the precision of the fitting.

One can then expand $\theta_i(\vec{p})$ to the first order

$$\theta_i(\vec{p}) = \theta_i(\vec{p}_o) + \vec{\nabla}\vec{\theta}_i \cdot \vec{\Delta p} \Big|_{\vec{p}=\vec{p}_o} \tag{5}$$

with $\vec{\Delta p} = \vec{p} - \vec{p}_o$. Equation (1) then becomes

$$\chi^2 = \sum_{i=1}^{N} \left(\frac{\theta_i^{exp} - \theta_i(\vec{p}_o) - \vec{\nabla}\vec{\theta}_i \cdot \vec{\Delta p} \Big|_{\vec{p}=\vec{p}_o}}{\Delta\theta_i^{exp}} \right)^2 \tag{6}$$

The solution $\vec{\Delta p}$ which minimizes χ^2 is given by (36):

$$\vec{\Delta p} = -\alpha^{-1} \vec{\nabla}\chi^2 \tag{7}$$

where α is the second derivative matrix (or error matrix).

The search for χ^2 minimum is thus carried out in the $-\vec{\nabla}\chi^2$ direction by replacing $\vec{p}_o$ by $\vec{p}_o + \vec{\Delta p}$ for each step in the iteration procedure. The minimum is achieved with $\vec{\Delta p} \to 0$. The errors of the parameters involved in such calculations are the square roots of the diagonal elements of the second derivative inverse matrix α^{-1}:

$$\delta_{pi} = \alpha_{ii}^{-1/2} \tag{8}$$

The results of each iteration, especially χ^2 and $|\vec{\nabla}\chi^2|^2$ are given and their convergence will show whether the input parameters and the line shape are of proper choice.

The MÖSSBR Memory

The parameters involved are the line positions, line heights and line widths.

Equation (2) is computed by the subroutine FUNC which calculates also its first and second derivatives. The iterations are performed through the subroutine CURFIT. The two subroutine EXAM and JACOBI are used to compute equation (7), and equation (8) is obtained by the subroutine MATINV.

A program called TRACEUR is used to plot by CALCOMP the experimental Mössbauer spectrum together with the one resulting from the curve-fitting.

```
      PROGRAM MOSSBR(INPUT,OUTPUT,TAPE5=INPUT,TAPE6=OUTPUT,TAPE99,PUNCH)
C
C                CURVE FITTING , LINE + LORENTZIANS
C     M          =NUMBER OF PARAMETERS
C     KG         =NUMBER OF LORENTZIANS UP TO SIX
C     L4         =NUMBER OF ITERATIONS ALLOWED
C     N0         =INITIAL CHANNEL OF THE GROUP
C     N          =NUMBER OF CHANNELS IN THE GROUP
C     B(3*KG+2)=SLOPE
C     B(3*KG+1)=BACKGROUND
C     B(3*J)    =CHANNEL NUMBER OF PEAK
C     B(3*J-1) =HALF WIDTH AT HALF MAXIMUM
      B(3*J-2) =HEIGHT OF THE PEAK
C
      DIMENSION Z(256),FM(256),FC(256),DF(256),ERR(256),B(20),B1(20),
     1B2(20,20),DC(2183),S(6),DAT(256),RUNNO(18),S1(6),P(6),PE(6),PH(6),
     2PHE(6),PW(6),PWE(6),A(6),AE(6),SAMPLE(72),ABC(2),Y(4),TIME(2),
     3DATA(256)
      COMMON/DATA/ABC,Y
      COMMON DC
      EQUIVALENCE (Z,DC),(FM,DC(257)),(FC,DC(513)),(DF,DC(769)),
     1(ERR,DC(1025)),(B1,DC(1281)),(B2,DC(1301)),(N,DC(1701)),
     2(L4,DC(1703)),(Q1,DC(1704)),(Q2,DC(1705)),(M,DC(1706)),
     3(B,DC(1719)),(I,DC(2180)),(L,DC(2179)),(KG,DC(2182))
      DATA(ABC=2HNO,3HYES),(Y=1H ,1HC,1H*,1HM)
C
C     READ IN SPECTRUM
C     DATA= MOSSBAUER DATA CORRECTED LATER FOR CURFIT
C     Q1 AND Q2 ARE THE PRECISIONS OF THE CURVE FITTING
C
      READ (5,7) Q1,Q2
    7 FORMAT(2F5.2)
      WRITE(6,8) Q1,Q2
    8 FORMAT (1X,4HQ1 = ,F5.2,5X,4HQ2 = ,F5.2)
 1000 READ(5,910) DAT
  910 FORMAT (12X,10F6.0)
      WRITE (6,188)
  188 FORMAT (1H1)
      WRITE(6,3)
    3 FORMAT(2X,13H INITIAL DATA//)
      WRITE(6,931)DAT
  931 FORMAT(13X,10F9.0)
      DO 9 I=2,255
      DD1=DAT(I-1)*0.75
      DD2=DAT(I-1)*1.25
      IF(DAT(I).GT.DD1.AND.DAT(I).LT.DD2) GO TO 9
      DAT(I)=(DAT(I-1)+DAT(I+1))/2.0
    9 CONTINUE
C
```

```
C
C     CALCULATE CORRECTED SPECTRUM DATA
C     CORRECTION FOR CHANGE IN SOLID ANGLE DURING DOPPLER MOTION
C     NC= QUARTER OF THE TOTAL NUMBER OF CHANNELS ON SPECTROMETER
C
      NC =64
       ALPHA1=(DAT(3*NC-1)+DAT(3*NC)+DAT(3*NC+1))/3.0
       ALPHA2=(DAT(NC-1)+DAT(NC)+DAT(NC+1))/3.0
       AN=SQRT(ALPHA1/ALPHA2)
       ALPHA=(AN-1.0)/(AN+1.0)
       YNC=NC
       DO 930 I=1,NC
       NC1=NC+I
       NC2=2*NC+I
       NC3=3*NC+I
       DAT(I)=DAT(I)*(1.0+ALPHA*FLOAT(I)/YNC)**2
       DAT(NC1)=DAT(NC1)*(1.0+ALPHA*FLOAT(NC-I)/YNC)**2
       DAT(NC2)=DAT(NC2)*(1.0-ALPHA*FLOAT(I)/YNC)**2
       DAT(NC3)=DAT(NC3)*(1.0-ALPHA*FLOAT(NC-I)/YNC)**2
  930  CONTINUE
      WRITE (6,4)
    4 FORMAT (5X,14HCORRECTED DATA//)
      WRITE(6,931)DAT
      WRITE (6,188)
C
C     RUNNO=PROVIDES 18 SPACES FOR SPECIFYING THE DATE OF EXPERIMENT
C     SAMPLE=PROVIDES 72 SPACES FOR SPECIFYING THE SAMPLE
C     TIME=PROVIDES 12 SPACES FOR SPECIFYING THE DURATION OF EXPERIMENT

      READ(5,1)RUNNO
    1  FORMAT(18A1)
      WRITE(6,2)RUNNO
    2 FORMAT (1X,14H RUN NUMBER=     ,18A1/)
       READ (5,220) SAMPLE
  220  FORMAT (72A1)
       WRITE (6,222) SAMPLE
  222  FORMAT(1X,14H SAMPLE     =   ,72A1/)
      READ (5,150) TIME
  150 FORMAT (2A6)
      WRITE(6,151) TIME
  151 FORMAT(1X,14H TIME       =   ,2A6/)
      READ (5,939) NO,N,KG,L4
  939 FORMAT (4I3)
      WRITE(6,10)NO,N,KG
   10 FORMAT(1X20H*INITIAL CHANEL=     I3,25H   *NUMBER OF CHANNELS=  I3,
     129H    NUMBER OF LORENTZIANS=    I2/)
      M=3*KG+2
```

```
      DO 115 I=1,N
      KNO=I+NO
      Z(I)=(KNO-1)
       FM(I)=DAT(KNO-1)
  115 ERR(I)=SQRT(FM(I))
      READ(5,89)B(3*KG+1)
89    FORMAT (1F8.0)
      WRITE(6,11)B(3*KG+1)
   11 FORMAT (1X14H BACKGROUND=  F8.0/)
      B(3*KG+2)=0.0
      READ (5,122) (B(3*J),J=1,KG)
  122 FORMAT(6F3.0)
      WRITE(6,12)(B(3*J),J=1,KG)
   12 FORMAT(1X,18H PEAK POSITIONS=  6(F15.0)/)
      READ (5,5) (B(3*J-2),J=1,KG)
    5 FORMAT(6F8.0)
      WRITE(6,13)(B(3*J-2),J=1,KG)
   13 FORMAT(1X,16H PEAK HEIGHTS=  6F15.0/)
      READ (5,120) (B(3*I-1),I=1,KG)
 120  FORMAT(6F5.3)
      WRITE(6,14)(B(3*I-1),I=1,KG)
   14 FORMAT(1X,9H SIGMA=  6F15.3///)
      DO 21 J=1,KG
   21 B(3*J-2)=B(3*J-2)*B(3*J-1)**2/10000.0
      B(3*KG+1)=B(3*KG+1)/10000.0
      DO 22 I=1,N
      FM(I)=FM(I)/10000.0
   22 ERR(I) = ERR(I)/10000.
      WRITE (6,1881)
 1881 FORMAT (39H0 CURVE FITTING         LINE+LORENTZIANS //)
      CALL CURFIT
      WRITE(6,188)
      WRITE (6,135)
  135 FORMAT(1X,11H PARAMETERS//3X,1HJ,10X,4HB(J),27X,6HERRORS//)
      WRITE (6,140)(J,B(J),B1(J),J=1,M)
  140 FORMAT(3X,I2,5X,E16.6,15X,E16.6 /)
       DO 200 I=1,KG
       P(I)=B(3*I)
       PE(I)=B1(3*I)
       PH(I)=10000.0*B(3*I-2)/B(3*I-1)**2
       T=2.0*(B1(3*I-1)/B(3*I-1))**2
       W=(B1(3*I-2)/B(3*I-2))**2
       PHF(I)=PH(I)*SQRT(T+W)
       PW(I)=2.0*B(3*I-1)
       PWE(I)=2.0*B1(3*I-1)
       A(I)=31415.9265*B(3*I-2)/B(3*I-1)
       TT=(B1(3*I-1)/B(3*I-1))**2
       WW=(B1(3*I-2)/B(3*I-2))**2
       AE(I)=A(I)*SQRT(TT+WW)
  200  CONTINUE
```

```
      WRITE(6,188)
       WRITE (6,201)
  201  FORMAT    (1X,15H LINE POSITIONS,6X,7H ERRORS/)
       WRITE (6,202) (P(I),PE(I),I=1,KG)
  202 FORMAT     (3X,1F10.5,6X,1F11.8/)
       WRITE (6,203)
  203 FORMAT (/,1X,13H LINE HEIGHTS,8X,7H ERRORS/)
       WRITE (6,204) (PH(I),PHE(I),I=1,KG)
  204 FORMAT(2X,F10.3,10X,F10.4/)
       WRITE (6,205)
  205  FORMAT (/,1X,14H FWHM OF LINES,7X,7H ERRORS/)
       WRITE (6,206) (PW(I),PWE(I),I=1,KG)
  206  FORMAT     (3X,1F10.6,6X,1F10.7/)
       WRITE (6,207)
  207  FORMAT (/,5X,11H LINE AREAS,8X,7H ERRORS/)
       WRITE (6,208) (A(I),AE(I),I=1,KG)
  208  FORMAT (1X,1F16.6,2X,1F16.6/)
      WRITE (6,188)
      CALL PLOTB(N0,N,FC,FM)
      DO  40 KK=1,N
      FC(KK) = FC(KK)*10000          $     FM(KK) = FM(KK)*10000
 40   CONTINUE
      WRITE(6,188)
      WRITE(6,935)   (FC(KJ),KJ=1,N)
      PUNCH 9481,N,N0
9481  FORMAT (5H≠≠≠N=,I5,5H/≠N0=,I5,2H//)
      PUNCH 935,     (FC(KJ),KJ=1,N)
      WRITE(6,935)   (FM(KJ),KJ=1,N)
 935  FORMAT ( 5F15.6  )
      PUNCH 935,     (FM(KJ),KJ=1,N)
      READ (5,16) JO
   16 FORMAT (I1)
      IF(JO-2) 1000,1001,1001
 1001 STOP
      END
```

```
      SUBROUTINE CURFIT
C          F O R T R A N  4
      DIMENSION Z(256),FM(256),FC(256),DF(256),ERR(256),X(256),
     1B(20),B1(20),B2(20,20),GRAD(20),D1(20),D2(20,20),DC(1403),B3(20,20
     2),AA(20),BB(20),W1(20),W2(20),ABC(2),B8(20,20),Y(4)
      COMMON/DATA/ABC,Y
      COMMON DC
      EQUIVALENCE (Z,DC),(FM,DC(257)),(FC,DC(513)),(DF,DC(769)),
     1(ERR,DC(1025)),(B1,DC(1281)),(B2,DC(1301)),(N,DC(1701)),
     2(L4,DC(1703)),(Q1,DC(1704)),(Q2,DC(1705)),(M,DC(1706)),
     3(B,DC(1719)),(GRAD,DC(1739)),(D1,DC(1759)),(D2,DC(1779)),
     4(I,DC(2180)),(L,DC(2179))
      DATA(ABC=2HNO,3HYES),(Y=1H ,1HC,1H*,1HM)
      L1 = 0
      SA = 0.0
      DO 1000 J=1,20
      B1(J)=0.0
      DO 1000 K=1,20
 1000 B2(J,K)=0.0
      DO 100 I = 1, N
      X(I) = ERR(I)**2
      L=1
      CALL FUNC(2)
      DF(I) =FM(I) - FC(I)
      DO 101 J=1,M
      B1(J)=B1(J)-(2.0*DF(I)*D1(J))/X(I)
      DO 101 K=1,M
  101 B2(J,K)=B2(J,K)-(2.0*(DF(I)*D2(J,K)-D1(J)*D1(K)))/X(I)
  100 SA = SA + DF(I)**2/X(I)
      GMOD=0.0
      DO 102 J=1,M
  102 GMOD=GMOD+B1(J)**2
      WRITE(6,243)SA,GMOD
  243 FORMAT (1X,26H*INITIAL VALUE SUM OF SQ.=E13.5,20X,17H*SQ MOD OF GR
     1AD =E13.5)
      WRITE(6,1751)
 1751 FORMAT(14H0 DERIVATIVES-)
      WRITE(6,240)(B1(J),J=1,M)
  240 FORMAT (15X,5(E13.5,8X)/)
      IF (SA - Q1) 110, 110, 200
  110 LE = 1
      GO TO 600
  200 S = 0.0
      GMOD = 0.0
      BMOD = 0.0
      PROD = 0.0
      A2=ABC(1)
      DO 210 J = 1, M
      B1(J) = 0.0
      DO 210 K = 1, M
  210 B2(J,K) = 0.0
```

```
      DO 220 I = 1, N
      L=1
      CALL FUNC(2)
      DF(I) = FM(I) - FC(I)
      DO 220 J = 1, M
      B1(J) = B1(J) - (2.0*DF(I)*D1(J))/X(I)
      DO 220 K = 1, M
  220 B2(J,K) = B2(J,K) - (2.0*(DF(I)*D2(J,K) -D1(J)*D1(K)))/X(I)
       DO 230 J = 1, M
  230 GRAD(J) = B1(J)
      L1 = L1 + 1
      CALL EXAM (B2,B1,M,LF)
      IF (LF)  250, 250, 305
  250 DO 231 II=1,M
      DO 231 JJ=1,M
  231 B3(II,JJ)=B2(II,JJ)
      CALL JACOBI (M,B3,1,NR,B2)
      DO 235 I=1,M
  235 B1(I)=B3(I,I)
      A2=ABC(2)
      DO 260 J = 1, M
  260 D1(J) = 0.0
      DO 270 J = 1, M
      DO 270 K = 1, M
  270 D1(K) = D1(K) + B2(J,K) *GRAD(J)
      DO 275 J = 1, M
      IF (B1(J))  280, 290, 285
  280 B1(J) = - B1(J)
  285 D1(J) = D1(J)/B1(J)
      GO TO 275
  290 D1(J) = 0.0
  275 CONTINUE
      DO 295 J = 1, M
  295 B1(J) = 0.0
      DO 300 J = 1, M
      DO 300 K = 1, M
  300 B1(J) = B1(J) + B2(J,K)*D1(K)
  305 DO 310 J=1,M
      GMOD = GMOD + GRAD(J)**2
      BMOD = BMOD + B1(J)**2
  310 PROD = PROD + GRAD(J)*B1(J)
      IF (GMOD - Q2)  315, 315, 320
  315 LE = 2
      GO TO 600
  320 C=PROD/SQRT(BMOD*GMOD)
      IF (C) 335, 335, 400
  335 LE = 4
      GO TO 600
  400 LD = 0
      L3 = 0
      DO 410 J = 1, M
  410 GRAD(J) = B(J) - B1(J)
  450 DO 420 I = 1, N
      L=2
      CALL FUNC (1)
      DF(I) = FM(I) - FC(I)
  420 S = S + DF(I)**2/X(I)
```

```
      IF (SA - S) 435, 500, 500
  435 LD = LD + 1
  430 DO440 J = 1, M
      B1(J) = B1(J)/2.0
  440 GRAD(J) = B(J) - B1(J)
      S = 0.0
      L3 = L3 + 1
      IF (L3 - 256) 450, 460, 460
  460 LE = 5
      GO TO 600
  500 IF (LD) 505, 505, 506
  506 LD = 0
      GO TO 430
  505 DO 510 J = 1, M
  510 B(J) = GRAD(J)
      SA = S
      IF (SA - Q1) 507, 507, 530
  507 LE = 1
      GO TO 600
  530 IF (L4) 200, 200, 900
  900 WRITE(6,920)L1,A2,L3,S,GMOD,(B(J),J=1,M)
  920 FORMAT(//,15H ITERATION NO.=I5,10X,43H   TRANSFORMATION MADE TO PR
     1INCIPAL AXES = A4,10X,   18H BINARY CHOP USED=I3,6H TIMES/1X,27H W
     2EIGHTED SUM OF SQUARES = E14.7,25X,32H   SQUARE MODULUS OF GRADIEN
     3T = E14.7/20H   PARAMETERS B(J) -/(6E17.8)/)
      IF (L1 - L4) 200, 910, 910
  910 LE = 6
      GO TO 600
  600 DO 710 J=1,M
      B1(J) = 0.0
      DO 710 K=1,M
  710 B2(J,K) = 0.0
      L=1
      DO 720 I = 1, N
      CALL FUNC(2)
      DF(I) = FM(I) - FC(I)
      DO 720 J = 1, M
      B1(J) = B1(J) - (2.0*DF(I)*D1(J))/X(I)
      DO 720 K = 1, M
  720 B2(J,K) = B2(J,K) - (2.0*(DF(I)*D2(J,K) -D1(J)*D1(K)))/X(I)
      CALL MATINV(B2,M,B1,1,DETERM)
      DO 730 J=1,M
      IF (B2(J,J)) 2001,2001,2002
 2001 B1(J) = -SQRT(-B2(J,J))
      GO TO 730
 2002 B1(J)= SQRT(B2(J,J))
  730 CONTINUE
      DO 740 J=1,M
      DO 740 K=1,M
  740 B2(J,K)=B2(J,K)/(B1(J)*B1(K))
      WRITE(6,551)LE,SA
  551 FORMAT(//,13H EXIT NUMBER=I3,20X,25H WEIGHTED SUM OF SQUARES=E15.8
     1//)
      RETURN
      END
```

```
      SUBROUTINE FUNC (LX)
      SUBROUTINE FUNC
      DIMENSION DC(2183),B(20,2),D1(20),D2(20,20),FC(256),Z(256),E(6)
      COMMON DC
      EQUIVALENCE (Z,DC),(FC,DC(513)),(B,DC(1719)),(D1,DC(1759)),
     1(D2,DC(1779)),(M,DC(1706)),(L,DC(2179)),(I,DC(2180)),(KG,DC(2182))
      DO 50 J=1,M
      D1(J)=0.0
      DO 50 K=1,M
   50 D2(J,K)=0.0
      FC(I)=B(M,L)*Z(I) + B(M-1,L)
      DO 60 J=1,KG
   60 FC(I)=FC(I) + B(3*J-2 ,L)/((Z(I)-B(3*J,L))**2 + B(3*J-1,L)**2)
      GO TO (110,120),LX
  120 D1(M-1)=1.0
      D1(M)=Z(I)
      DO 70 J=1,KG
      XI=(Z(I)-B(3*J,L))**2
      ETA=B(3*J-1,L)**2
      DEN=XI+ETA
      D1(3*J-2)=1.0/DEN
      D1(3*J-1)=-2.0*B(3*J-1,L)*B(3*J-2,L)/DEN**2
      D1(3*J)=2.0*(Z(I)-B(3*J  ,L))*B(3*J-2,L)/DEN**2
      D2(3*J-1,3*J-2)=-2.0*B(3*J-1,L)/DEN**2
      D2(3*J-2,3*J-1)=D2(3*J-1,3*J-2)
      D2(3*J,3*J-2)=2.0*(Z(I)-B(3*J,L))/DEN**2
      D2(3*J-2,3*J) = D2(3*J,3*J-2)
      D2(3*J-1,3*J-1)=-2.0*B(3*J-2,L)*(XI -3.0*ETA)/DEN**3
      D2(3*J-1,3*J)=-8.0*B(3*J-2,L)*B(3*J-1,L)*(Z(I)-B(3*J,L))/DEN**3
      D2(3*J,3*J-1)=D2(3*J-1,3*J)
   70 D2(3*J,3*J)=2.0*B(3*J-2,L)*(3.0*XI-ETA)/DEN**3
  110 CONTINUE
      RETURN
      END
```

```
      SUBROUTINE EXAM(A,B,M,LF)
C     SUBROUTINE EXAM                    -67-
        F O R T R A N  4
      DIMENSION A(20,20),B(20),C(20)
      DO 80 J=1,M
   80 C(J)=A(J,J)
      IF(A(1,1)) 60,200,70
   60 A(1,1) =-SQRT(-A(1,1))
      GO TO 300
   70 A(1,1) =SQRT(A(1,1))
      GO TO 100
  100 IF(M-1)400,400,110
  110 DO 115 K=2,M
  115 A(1,K)=A(1,K)/(A(1,1)          )
      DO 120 J=2,M
      J1=J-1
      S=A(J,J)
      DO 125 L=1,J1
  125 S=S-A(L,J)**2
      IF (S) 50,200,40
   50 A(J,J) =-SQRT(-S)
      GO TO 300
   40 A(J,J) =SQRT(S)
      GO TO 130
  130 IF(J-M)135,400,400
  135 J2=J+1
      DO 120 K=J2,M
      S=A(J,K)
      DO 145 L=1,J1
  145 S=S-A(L,J)*A(L,K)
  120 A(J,K)=S/A(J,J)
  400 B(1)=B(1)/A(1,1)
      IF(M-1)420,420,405
  405 DO 410 J=2,M
      S=B(J)
      J1=J-1
      DO 415 L=1,J1
  415 S=S-A(L,J)*B(L)
  410 B(J)=S/A(J,J)
  420 B(M)=B(M)/A(M,M)
      J=M-1
  435 IF(J)450,450,425
  425 S=B(J)
      J2=J+1
      DO 430 L=J2,M
  430 S=S-A(J,L)*B(L)
      B(J)=S/A(J,J)
      J=J-1
      GO TO 435
  450 LF=1
      GO TO 460
  200 LF=0
      GO TO 460
  300 LF=-1
  460 DO 465 J=1,M
      A(J,J)=C(J)
      IF(J-M)470,475,475
  470 J2=J+1
      DO 465 K=J2,M
  465 A(J,K)=A(K,J)
  475 RETURN
      END
```

```
      SUBROUTINE MATINV(A,N,B,M,DETERM)
C     SUBROUTINE MATINV
C       F O R T R A N  4
C     MATRIX INVERSION WITH ACCOMPANYING SOLUTION OF LINEAR EQUATIONS
      DIMENSION IPIVOT(20),A(20,20),B(20,1),INDEX(20,2),PIVOT(20)
      EQUIVALENCE (IROW,JROW),(ICOLUM,JCOLUM),(AMAX,T,SWAP)
      DETERM=1.0
      DO 20 J=1,N
   20 IPIVOT(J)=0
      DO 550 I=1,N
      AMAX=0.0
      DO 105 J=1,N
      IF(IPIVOT(J)-1)60,105,60
   60 DO 100 K=1,N
      IF(IPIVOT(K)-1)80,100,740
   80 IF(ABS(AMAX)-ABS(A(J,K)))85,100,100
   85 IROW=J
      ICOLUM=K
      AMAX=A(J,K)
  100 CONTINUE
  105 CONTINUE
      IPIVOT(ICOLUM)=IPIVOT(ICOLUM)+1
      IF (IROW-ICOLUM)140,260,140
  140 DETERM=-DETERM
      DO 200 L=1,N
      SWAP=A(IROW,L)
      A(IROW,L)=A(ICOLUM,L)
  200 A(ICOLUM,L)=SWAP
      IF(M)260,260,210
  210 DO 250 L=1,M
      SWAP=B(IROW,L)
      B(IROW,L)=B(ICOLUM,L)
  250 B(ICOLUM,L)=SWAP
  260 INDEX(I,1)=IROW
      INDEX(I,2)=ICOLUM
      PIVOT(I)=A(ICOLUM,ICOLUM)
      DETERM=DETERM*PIVOT(I)
      A(ICOLUM,ICOLUM)=1.0
      DO 350 L=1,N
  350 A(ICOLUM,L)=A(ICOLUM,L)/PIVOT(I)
      IF(M)380,380,360
  360 DO 370 L=1,M
  370 B(ICOLUM,L)=B(ICOLUM,L)/PIVOT(I)
  380 DO 550 L1=1,N
      IF (L1-ICOLUM)400,550,400
  400 T=A(L1,ICOLUM)
      A(L1,ICOLUM)=0.0
      DO 450 L=1,N
  450 A(L1,L)=A(L1,L)-A(ICOLUM,L)*T
      IF(M)550,550,460
  460 DO 500 L=1,M
  500 B(L1,L)=B(L1,L)-B(ICOLUM,L)*T
  550 CONTINUE
```

```
      DO 710 I=1,N
      L=N+1-I
      IF(INDEX(L,1)-INDEX(L,2))630,710,630
  630 JROW=INDEX(L,1)
      JCOLUM=INDEX(L,2)
      DO 705 K=1,N
      SWAP=A(K,JROW)
      A(K,JROW)=A(K,JCOLUM)
      A(K,JCOLUM)=SWAP
  705 CONTINUE
  710 CONTINUE
  740 RETURN
      END
```

```
      SUBROUTINE JACOBI (N,Q,JVEC,M,V)
C     SUBPROGRAM FOR DIAGONALIZATION OF MATRIX Q BY SUCCESSIVE ROTATIONS
      DIMENSION Q(20,20),V(20,20),X(20),IH(20)
C
C     NEXT 8 STATEMENTS FOR SETTING INITIAL VALUES OF MATRIX V
C
      IF(JVEC) 10,15,10
   10 DO 14 I=1,N
      DO 14 J=1,N
      IF(I-J) 12,11,12
   11 V(I,J)=1.0
      GO TO 14
   12 V(I,J)=0.
   14 CONTINUE
C
   15 M=0
      NEXT 8 STATEMENTS SCAN FOR LARGEST OFF DIAG. ELEM. IN EACH ROW
C     X(I) CONTAINS LARGEST ELEMENT IN ITH ROW
C     IH(I) HOLDS SECOND SUBSCRIPT DEFINING POSITION OF ELEMENT
C
      MI=N-1
      DO 30 I=1,MI
      X(I)=0.
      MJ=I+1
      DO 30 J=MJ,N
      IF (X(I)-ABS (Q(I,J))) 20,20,30
   20 X(I)=ABS (Q(I,J))
      IH(I)=J
   30 CONTINUE
C
C     NEXT 7 STATEMENTS FIND FOR MAXIMUM OF X(I)S FOR PIVOT ELEMENT
   40 DO 70 I=1,MI
      IF(I-1) 60,60,45
   45 IF (XMAX-X(I)) 60,70,70
   60 XMAX=X(I)
      IP=I
      JP=IH(I)
   70 CONTINUE
C
C     NEXT 2 STATEMENTS TEST FOR XMAX,IF LESS THAN 10**-8,GO TO 1000

      EPSI=1.E-8
      IF (XMAX-EPSI) 1000,1000,148
C
  148 M=M+1
C
```

```
C     NEXT 11 STATEMENTS FOR COMPUTING TANG,SINE,COSN,Q(I,I),Q(J,J)
C
      IF (Q(IP,IP)-Q(JP,JP)) 150,151,151
  150 TANG =-2.*Q(IP,JP)/(ABS(Q(IP,IP)-Q(JP,JP))+SQRT((Q(IP,IP)-Q(JP,JP)
     1)**2+4.*Q(IP,JP)**2))
      GO TO 160
  151 TANG =+2.*Q(IP,JP)/(ABS(Q(IP,IP)-Q(JP,JP))+SQRT((Q(IP,IP)-Q(JP,JP)
     1)**2+4.*Q(IP,JP)**2))
  160 COSN=1.0/SQRT(1.0+TANG**2)
      SINE=TANG*COSN
      QII= Q(IP,IP)
      Q(IP,IP)= COSN**2*(QII+TANG*(2.*Q(IP,JP)+TANG*Q(JP,JP)))
      Q(JP,JP)= COSN**2*(Q(JP,JP)-TANG*(2.*Q(IP,JP)-TANG*QII))
C
      Q(IP,JP)=0.
C
C     NEXT 4 STATEMENTS FOR PSEUDO RANK OF THE EIGENVALUES
      IF (Q(IP,IP)-Q(JP,JP)) 152,153,153
  152 TEMP=Q(IP,IP)
      Q(IP,IP)=Q(JP,JP)
      Q(JP,JP)=TEMP
C
C     NEXT 6 STATEMENTS ADJUST SIN,COS FOR COMPUTATION OF Q(I,K),V(I,K)
C
      IF(SINE) 154,155,155
  154 TEMP=+COSN
      GO TO 170
  155 TEMP=-COSN
  170 COSN=ABS(SINE)
      SINE=TEMP
C
C     NEXT 10 STATEMENTS FOR INSPECTING  THE I≠S BETWEEN I+1 AND N-1 TO
C     DETERMINE WHETHER A NEW MAXIMUM VALUE SHOULD BE COMPUTED SINCE
C     THE PRESENT MAXIMUM IS IN THE I OR J ROW
C
  153 DO 350 I=1,MI
      IF (I-IP) 210,350,200
  200 IF (I-JP) 210,350,210
  210 IF (IH(I)-IP) 230,240,230
  230 IF (IH(I)-JP) 350,240,350
  240 K= IH(I)
      TEMP=Q(I,K)
      Q(I,K)=0.
      MJ=I+1
      X(I)=0.
C
C     NEXT 5 STATEMENTS SEARCH IN DEPLETED ROW FOR NEW MAXIMUM
C
      DO 320  J=MJ,N
      IF (X(I)-ABS(Q(I,J))) 300,300,320
  300 X(I)=ABS(Q(I,J))
      IH(I)=J
  320 CONTINUE
      Q(I,K)=TEMP
  350 CONTINUE
C
```

```
      X(IP)=0.
      X(JP)=0.
C
C     NEXT 30 STATEMENTS FOR CHANGING THE OTHER ELEMENTS OF Q
C
      DO 530 I=1,N
C
      IF (I-IP) 370,530,420
  370 TEMP=Q(I,IP)
      Q(I,IP)=COSN*TEMP+SINE*Q(I,JP)
      IF (X(I)-ABS(Q(I,IP))) 380,390,390
  380 X(I)=ABS(Q(I,IP))
      IH(I)=IP
  390 Q(I,JP)=-SINE*TEMP+COSN*Q(I,JP)
      IF (X(I)-ABS(Q(I,JP))) 400,530,530
  400 X(I)=ABS(Q(I,JP))
      IH(I)=JP
      GO TO 530
C
  420 IF (I-JP) 430,530,480
  430 TEMP =Q(IP,I)
      Q(IP,I)=COSN*TEMP+SINE*Q(I,JP)
      IF (X(IP)-ABS(Q(IP,I))) 440,450,450
  440 X(IP)=ABS(Q(IP,I))
      IH(IP)=I
  450 Q(I,JP)=-SINE*TEMP+COSN*Q(I,JP)
      IF (X(I)-ABS(Q(I,JP))) 400,530,530
C
  480 TEMP=Q(IP,I)
      Q(IP,I)=COSN*TEMP+SINE*Q(JP,I)
      IF(X(IP)-ABS(Q(IP,I))) 490,500,500
  490 X(IP)=ABS(Q(IP,I))
      IH(IP)=I
  500 Q(JP,I)=-SINE*TEMP+COSN*Q(JP,I)
      IF (X(JP)-ABS(Q(JP,I))) 510,530,530
  510 X(JP)=ABS(Q(JP,I))
      IH(JP)=I
  530 CONTINUE
C
C     NEXT 6 STATEMENTS TEST FOR COMPUTATION OF EIGENVECTORS
C
      IF (JVEC) 540,40,540
  540 DO 550 I=1,N
      TEMP=V(I,IP)
      V(I,IP)= COSN*TEMP+SINE*V(I,JP)
  550 V(I,JP)=-SINE*TEMP+COSN*V(I,JP)
      GO TO 40
 1000 RETURN
      END
```

```
      SUBROUTINE PLOTB (N0,N,AA,BB)
C     SUBROUTINE PLOT B
C     A= LARGEST OF FC AND FM, B= SMALLEST
      DIMENSION X(116),AA(512),BB(512),Y(4),ABC(2)
      COMMON/DATA/ABC,Y
      DATA(ABC=2HNO,3HYES),(Y=1H ,1HC,1H*,1HM)
      A=AA(1)
      B=A
      DO 900 I=1,N
      IF(AA(I)-A)905,905,910
  910 A=AA(I)
  905 IF(BB(I)-A)915,915,920
  920 A=BB(I)
  915 IF(AA(I)-B)930,925,925
  930 B=AA(I)
  925 IF(BB(I)-B)935,900,900
  935 B=BB(I)
  900 CONTINUE
      FACTOR = 1.0
  520 IF (A-B-1000.0) 500, 510, 510
  500 A = 2.0*A
      B = 2.0*B
      FACTOR = 2.0*FACTOR
      GO TO 520
  510 KD = (A-B)/112.0 + 1.0
      KS = IFIX(B) - 2*KD
      WRITE (6,1)
    1  FORMAT(119H0...0.........1.........2.........3.........4.........
     15.........6.........7.........8.........9.........10........11...)
      DO 100 I=1,N
      DO 110 K=1,116
  110 X(K)=Y(1)
      K = AA(I)*FACTOR
      K = (K-KS)/KD
      X(K) = Y(2)
      L = BB(I)*FACTOR
      L = (L-KS)/KD
      IF(L-K)120,130,120
  130 X(L)=Y(3)
      GO TO 105
  120 X(L)=Y(4)
  105 IN0=I+N0-1
  100 WRITE (6,90)IN0,X
   90 FORMAT(1X13,116A1)
      WRITE (6,1)
      RETURN
      END
```

```
      PROGRAM  TRACEUR (INPUT,OUTPUT,TAPE99,TAPE60=INPUT)

      COMMON / NUM /        NGRAF,NSYMB,MESSAJ( 7),CALC,MES
      DIMENSION  FC(256),FM(256)
      LOGICAL  CALC,MES

C     NSYMB = TOTAL NUMBER OF SPACES OF MESSAJ
C     MESSAJ = TITLE OF THE GRAPH
C     IDENTIFY PLOTTER OUTPUT
C
      CALL NAMPLT
C
      ETABLISH NEW ORIGIN AT LOWER LEF-HAND SIDE OF AVAILABLE PLOT AREA
C
      CALL PLOT (0.0,-0.5,-3)
C
 52   READ 11, NGRAF,NSYMB,MESSAJ,CALC,MES
      IF ( EOF,60)  50, 51
 51   PRINT 20
      READ 10,  N,N0
      PRINT 10, N,N0
      IF ( CALC )  53, 54
 53   READ 935,      (FC(KJ),KJ=1,N)
      PRINT 935,     (FC(KJ),KJ=1,N)
 54   IF ( MES )  55, 56
 55   READ 935.      (FM(KJ),KJ=1,N)
      PRINT 935,     (FM(KJ),KJ=1,N)
 56   IF ( CALC.OR.MES )  CALL  TRACE (FC,FM,N0,N)
      GO TO  52
 50   CALL ENDPLT

 10   FORMAT ( 2(5X,I5)  )
 11   FORMAT ( 2I5,6A10,A8,2L1    )
 20   FORMAT ( 1H1, 5(/)    )
 935  FORMAT ( 5F15.6  )

      END  TRACEUR
```

```
      SUBROUTINE TRACE(FC,FM,N0,N)
X
C
C     SUBROUTINE FOR PLOTTING EXPERIMENTAL AND COMPUTED
C      MOSSBAUER SPECTRA
C
      COMMON / NUM /        NGRAF,NSYMB,MESSAJ( 7),CALC,MES
      DIMENSION FC(256),FM(256),X(258),Y(258,2),TEMPO(4)
      LOGICAL  CALC,MES
C
CC    GENERATE PLOT DATA
C
      DO 40  I=1,N
      IF ( CALC )  53, 54
 54   Y(I,1) = Y(I,2) = FM(I)      $    GO TO  057
 53   IF ( MES )  55, 56
 56   Y(I,2) = Y(I,1) = FC(I)      $    GO TO  057
 55   Y(I,1) = FC(I)               $    Y(I,2) = FM(I)
057   IN0 = I+ N0-1
      GO TO (501,502,503,504,505,506,507,508,509,510,511) ,NGRAF
C     INSERT EQ. OF CALIBRATION INTO STATEMENT OF NGRAF
 501  X(I) =0.0738*IN0-9.2330
      GO TO  040
  502 X(I)=0.0335*IN0-4.0691
      GO TO  040
  503 X(I)=0.0335*IN0-4.0691
      GO TO  040
  504 X(I) = 0.0346*IN0-4.2058
      GO TO  040
  505 X(I) = 0.0346*IN0-4.2058
      GO TO  040
  506 X(I) = 0.0177*IN0-2.0307
      GO TO  040
  507 X(I)=0.0335*IN0-4.0691
      GO TO  040
 508  CONTINUE
      GO TO  040
 509  CONTINUE
      GO TO  040
 510  CONTINUE
      GO TO  040
 511  CONTINUE
      GO TO  040
040   CONTINUE
C
```

```
C
C       FIND MIN. AND MAX. TO DETERMINE COMMON  SCALE
C
        TEMPO = TEMPO(2) = Y
        DO 041   I=1,N
        DO 041   J=1,2
        IF ( Y(I,J)-TEMPO(1)   )  50, 051, 051
 50     TEMPO(1) = Y(I,J)
        GO TO  041
051     IF ( Y(I,J)-TEMPO(2)   )  041, 041, 52
 52     TEMPO(2) = Y(I,J)
041     CONTINUE
C
C       CALL SCALE FOR PROPER SCALING OF AXES
C
        CALL SCALE1(X,8.0,N,1,25.0)
        CALL SCALE1(TEMPO,5.0,2,1,20.0)
        N1=N+1                          $     N2 = N+2
        Y(N1 ,1) = Y(N1 ,2) = TEMPO(3)
        Y(N2 ,1) = Y(N2 ,2) = TEMPO(4)
C
C       DRAW THE X AND THE Y AXIS
C
        CALL AXIS1(2.0,3.0,16HVELOCITY(MM/SEC),-16,8.0,0.0,X(N1),X(N2),25.
       10)
        CALL AXIS1(2.0,3.0,6HCOUNTS,+6,5.0,90.0,TEMPO(3),TEMPO(4),20.0 )
C
        LABEL GRAPH
C
        CALL SYMBOL(2.2,2.0,0.2,MESSAJ,0.0,NSYMB)
C
C       ETABLISH NEW ORIGIN AT INTERSECTION OF AXES
C
        CALL PLOT(2.0,3.0,-3)
C       DRAW EXPERIMENTAL AND CALCULATED SPECTRA
        IF ( CALC )  CALL  LINE (X,Y(1,1),N,1,0,0)
        IF ( MES  )  CALL  LINE (X,Y(1,2),N,1,-1,1)
C
C       MOVE PEN FROM PLOT AREA AND SIGN OFF
C
        CALL PLOT(10.0,-3.0,-3)
        RETURN
        END  TRACE
```

REFERENCES

(1) Mössbauer,R.L., Z. Physik 151,124 (1958).

(2) Mössbauer,R.L., Naturwissenshaften 45, 538(1958).

(3) Pound, R.V., Rebka Jr., G.A., Phys. Rev. Letters 4, 337 (1960).

(4) Mitra, S.S., Singh, R.S., Phys. Rev. Letters 16,694(1966)

(5) Singh,P.P., Rivest, R., Can. J. Chem. 46, 1773(1968).

(6) Obenshain, F.E., Wigener, H.H.F., Phys. Rev. 121,1344 (1961).

(7) DeVoe, J.R., and Spijkerman,J.J., Analytical Chem. 40, 472R (1968).

(8) Goldanskii, V.I., Makarov, E.F., Chem. Applications of Mössbauer spectroscopy, Acad. Press,N.Y. (1968).

(9) Lamb Jr., W.E., Phys. Rev. 55, 190 (1939).

(10) Muir, A.H., Atomic Int. Report, AI-6699 (1961).

(11) Holm, M.W., "Debye Characteristic Temperatures", Philips Petroleum Co. Report IDO-16399, Office of Tech. Serv., U.S. Dept. of Commerce, Washington 25,D.C.

(12) Mössbauer, R.L., Clauser, M.J., "Hyperfine Interaction" 506, Acad. Press, N.Y. (1967).

(13) Shirley, D.A., Kaplan, M., Axel, P., Phys. Rev. 123, 816 (1961).

(14) Vissher, W.M., (unpublished notes), Los Alamos Scientific Laboratory, Los Alamos, New Mexico.

(15) Tzara,C.,Barloutaud,R.,Phys. Rev. Letters 4,405(1960).

(16) Fermi, E., Segrè, E., Z. Physik 82, 729 (1933).

(17) Shirley, D.A., Rev. Mod. Phys. 36, 339 (1964).

(18) Walker, L.R., Wertheim, G.K., Jaccarino, V., Phys. Rev. Letters 6, 98 (1961).

(19) Pauling, L., "Nature of the Chemical Bond",Univ. Press N.Y. (1960).

(20) Wegener, H.H.F.,"Der Mössbauer Effekt und seine Anwendung in der Physik und Chemie." Mannheim, Germany (1965).

(21) Goldanskii, V.I., "The Mössbauer effect and its application to Chemistry." At. Energy Rev. 1, 3(1963).

(22) Danon, J.,"Applications of the Mössbauer effect in Chemistry and Solid State Physics.", Tech. Rept. Ser. Inter. At. Energy Agency 50, 89 (1966).

(23) Goldanskii, V.I., Makarov, E.F., and Stukan, R.A., Teor. i Eksperim. Khim. Akad. Nauk Ukr. SSR 2, 504 (1966).

(24) Šimaneck, E., and Šroubeck, Z.,Phys. Rev.163, 275 (1967).

(25) Duncan, J.F., and Wigley, P.W.R., J. Chem. Soc. 1963, 1120 (1963).

(26) Hanna, S.S., Heberle, J., Littlejohn, C., Perlow,G.J., Preston, R.S., and Vincent, D.H., Phys. Rev. Letters 4, 177 (1960).

(27) Wertheim, G.K., "Mössbauer effect, Principles and Applications.", Acad. Press,N.Y. (1964).

(28) Watson, R.E., Freeman, A.J., Proc. Intern. Conf. on Mössbauer effect, 2nd, Saclay (France),1961, Wiley, N.Y. (1962).

(29) Collins, R.L., and Travis, J.C.,"Mössbauer effect Methodology.", vol. 3, Plenum Press,N.Y. (1967).

(30) Matthias,E., Schneider, W., and Steffen, R.M., Phys. Rev. 125, 261 (1962).

(31) DeBenedetti, S., Barros, F.D.,and Hoy, G.R., Annual Rev. of Nucl. Sc. 16, 31 (1966).

(32) Herber,R.H., "Mössbauer effect Methodology.", vol.1, Plenum Press, N.Y. (1965).

(33) Ingalls, R., Phys. Rev. 133, A787 (1964).

(34) Abragam, A., and Boutron, F., Compt. Rend. 252, 2404 (1961).

(35) Freeman, A.J., and Watson, R.E., Phys. Rev. 131, 2566 (1963).

(36) Arndt, R.A., and Mac Gregor, M.H., Methods in Computational Physics, Acad. Press,vol.6, 251(1966).